FACULTY OF SCIENCE
UNIVERSITY OF COPENHAGEN

ENTANGLEMENT PURIFICATION FOR CONTINUOUS VARIABLE PHOTONIC STATES

MADS LYKKE ANDERSEN

SUPERVISOR: ANDERS SØNDBERG SØRENSEN

A Thesis Presented for the Degree of
Cand. Scient. in Physics

Niels Bohr Institute
University of Copenhagen
Denmark

February 15, 2007

Foreword

In august 2005 I decided that I wanted to write my masterthesis in the field of theoretical quantum optics. I walked to the office of Anders Sørensen and stated my interest.

Anders presented a range of ideas and I took particularly interest in the one that at a later point in time would become this thesis. It was a proposal for a continuous variable purification protocol that would mimic the behavior of a known successful qubit purification protocol. A lot of reading of books and papers, and simulations in Mathematica followed. I would estimate that my time has been close to evenly distributed between reading, simulating and writing. During this work I also took time to be an instructor in classical mechanics 1 & 2, take on a job as chairman of my dorm for one semester and undertake a long journey to Vietnam. These explorations have all been personally rewarding although time-consumming, the result is that I now, 1 1/2 year later, am ready to turn in my thesis.

Working with this masterthesis have been a great learning process. If I were to start over today I would probably have done many things differently, but I guess that things always seems easier looking backwards in time. I fell, that I now am capable of finding my own way in a scientific field and have found great joy in exploring the world of quantum optics. It is a field with many talented people in rapid development.

I would like to thank my supervisor, Anders Søndberg Sørensen. Without him there would not have been a thesis, in this thesis I explore an idea originally formulated by Anders. I would like to thank Anders for being patient with me, especially at the times where I was preoccupied with other things. Throughout the year Anders always had time to talk and help, and he was always able to provide an answer when I was in need of one, this is a great ability for a supervisor.

I would also like to thank Peter Ahlgren for keeping me company throughout the many late nights spent finishing this thesis at my desk at the top of the Niels Bohr Institute. Rasmus Toft-Petersen has taken time to read through the hole thesis commenting on everything from nomenclature to understanding, for this I am very thankful. Finally I want to mention my girlfriend, Signe Juulskov Poulsen. She has been a great support

throughout the project, she has provided me with much optimism and encouragement. I owe her a big bouquet of flowers.

I have chosen to write this thesis to a large extent in a “we” form: “We find that”, “we can see” and so fourth. The reason for this choice is to include the reader in the process. When I write that “we calculate that $2 + 2 = 4$” then I mean for you (the reader), to sit by my side and agree or disagree with me when I state that $2 + 2 = 4$. The hope is that the reader will feel included in the calculations.

I hopefully suspect that you (the reader) will learn from- and enjoy reading this thesis, I certainly have done both, while I was writing it.

Respectfully yours,

Mads Lykke Andersen
February 15, 2007- Niels Bohr Institute - Copenhagen

Contents

Chapter 1

Motivation and Introduction

1.1 Motivation

In 1935, Einstein, Podolsky and Rosen (EPR) [1] wrote that if ”local realism” is taken for granted, then quantum theory is an incomplete description of the physical world. Local realism states; that if A and B are spacelike separated regions, then what happens in A cannot have a causal influence on what happens in B. Any sane grownup would agree in this statement, so it seemed like a real problem to quantum mechanics.

The EPR argument saw renewed attention in 1964 when John Bell wrote down his now famous inequalities [2, 3] that would make it possible to test if the world obeyed the laws of quantum mechanics or if it really is “local realistic“. Bell’s inequality states that there is an upper boundary for the correlations achievable for a hidden variable system.

The experiments that first tested Bell’s inequality were done by A. Aspect et al. [4, 5, 6] in 1981. In the abstract it says *”Our results, in excellent agreement with quantum mechanical predictions, strongly violate the generalized Bell’s inequalities, and rule out the whole class of realistic local theories“*. Aspect thus proved that quantum mechanics were right, and that the world truly is non-local.

Instead of seeing the non-local interaction as an possible inconsistency in quantum mechanics, they were seen as a new quantum phenomenon with new possibilities to be explored. The concept of entanglement was born.

A new field emerged at the borderline between physics and computer science, referred to as quantum information theory, it deals with a computer based on quantum mechanics - a quantum computer.

Quantum information theory was founded with the realization that information encoded in a quantum system could be manipulated in ways that would make otherwise intractable problems feasible to solve. The problem of finding the factors in a product of

two large unknown primes is one such problem. The fact that this is difficult is utilized when banks, public authorities and you and I share secret information over the internet. So it drew much attention when P. Shor [7] showed that it was possible to solve the problem of factorizing primes using a quantum computer in a reasonably time, as this blows open a huge security hole.

The physical implementation of a large scale quantum computer is very difficult, due to the harsh requirements to isolation of the quantum systems, low noise level and efficient and controlable interactions. It has been experimentally possible to implement the different parts separately, but the first quantum computer has yet to be built.

In the quantum computer of the future, quantum information needs to be moved from one place to another. This can be done with a teleportation protocol, but we need a reliable source of entanglement to implement this. Entangled photonic states provides an easy and fast way of distributing entanglement within and between quantum computers. It is crucial for the success of the quantum computations, that the utilized entanglement is good. Decoherence and noise inevitable destroys entanglement so we need a way to obtain better entanglement from partly broken entanglement. This is the problem that a entanglement purification procedure aims to solve.

1.2 Introduction

In this thesis we will set out to construct an entanglement purification protocol for continuous variable photonic states. We will try to purify the continuous variable entangled states that were presented by Garcia-Patron et al. [8], these state exhibit a high degree of entanglement, making them and interesting alternative to qubit states.

We will implement the purification by using beamsplitters and homodyne measurements of the quadrature phases. We will do this trying to mimic the behavior of a known purification protocol for qubits, which were suggested by Deutsch et al. [9].

We will use Wigner functions to describe the continuous variable photonic states. Wigner functions are easy to manipulate when we implement phase shifters, beamsplitters and homodyne detection. Even though the Wigner function transform in a simple way, they tend to involve many terms and huge expressions. We therefore need to do the calculations and simulations on a computer. The parameter space for the purified states are huge, we will use the simulations to find the effect of varying the different parameters. We will try to find an optimal set of parameters.

All the simulations in this thesis are done in Mathematica, the programs used in this process are presented in appendix D. Some of the plots presented in this thesis are bor-

rowed from other research works, when this is the case it is always explicitly stated. The majority of the plots in this thesis are produced using Mathematica and gnu-plot. Figures are done using X-fig, and for typesetting of this thesis LaTeX has been used.

Thesis outline

The thesis is divided into eight chapters with the following structure.

Chapter 1 - Motivation and Introduction This is the chapter that you are reading now. It presents the motivation for doing this thesis and give a short introduction to the field of quantum optics. An outline of the thesis is also given.

Chapter 2 - Theoretical background Provides the reader with the necessary background knowledge of quantum mechanics, Bell's inequality and quantum optics.

Chapter 3 - Quantum information Introduces the field of quantum information, gives examples of quantum computation and quantum simulation. Qubits are introduced along with the concepts of decoherence and purification. A comparison of qubits and continuous variables is also included.

Chapter 4 - Wigner functions Wigner functions are introduced as the description we will use for quantum light states. The Wigner function of a Gaussian state in presented along with some mathematical identities of Wigner functions that will prove usefull.

Chapter 5 - Preparation of the state Presents a way of preparing a state that is capable of breaking Bell's inequality in a loophole free manner. The properties of this state are subjected to detailed calculations. We will denote the state the two mode photon subtracted (TMPS) state.

Chapter 6 - Purification procedure Explains that the state we found in chapter 5 is analogous to a $|\phi^+\rangle$ Bell state. We present a qubit purification method for the $|\phi^+\rangle$ state and develop a continuous variable version of this, which should purify the TMPS state found in chapter 5.

Chapter 7 - The purified state Detailed calculations are done on the resulting state from the purification method. We compare the results found in this chapter to the results found for the TMPS state.

Chapter 8 - Conclusion and Outlook Concludes on the results found throughout the thesis and presents an outlook from this work.

Chapter 2

Theoretical background

The field of Quantum Optics (QO) provides a quantum mechanical description of light and the interactions between light and matter. The field has produced many great results and philosophical realizations, among these are the MASER and the LASER phenomenons, Dobbler cooling, optical tweezers and Bose-Einstein condensates. Other remarkable feats include quantum entanglement, quantum teleportation and recently the field has merged with theoretical computer science to produce the field of Quantum Information (QI).

The language of quantum optics is that of quantum mechanics, and everyone with a desire to venture into this field should have a elementary understanding of the concepts of quantum mechanics. The purpose of this chapter, is to provide the reader with the theoretical background necessary to understand the fundamental concepts of the tools we will be using throughout this thesis.

The reader is assumed to have a basic understanding of quantum mechanics and be familiar with the bra-ket formulation. All of the claims of this chapter can be found in the literature, e.g. [10, 11, 12, 13, 14], presenting proofs will therefore not be the main focus of this chapter although they are not everywhere omitted.

This chapter is not meant as a consistent derivation of various properties of quantum mechanical and quantum optical operators, but a guide to what concepts that are most important to this thesis.

2.1 Quantum mechanics

2.1.1 Notation

A word on notation is in order before we begin. Throughout this thesis we will not use multiple integral signs $\int dx \int dy \int dz$ or $\int\int\int dxdydz$ but just the form $\int dxdydz$, and the limits of integration are always from $-\infty \ldots \infty$ unless otherwise specified.

Quantum mechanical operators are provided with a hat $\hat{O}$ and expectancy values and averages of an operator $\hat{O}$ is given by $\langle\hat{O}\rangle$. The functions $\delta(x)$ and δ_{ij} denotes the Dirac and Kronecker deltafunctions respectively.

2.1.2 Pure and mixed states

Suppose a given quantum state cannot be described using a single state vector, but rather each statevector from a set $\{|\psi\rangle_i\}$ is known to occur with probability p_i, where $\sum_i p_i = 1$. If this is the case and more than one p_i is different from zero, then the system is described as a statistical mixture of states, and is called a mixed state.

A pure state on the other hand is describable with a single state vector, that is, if there exist a j such that $p_i = \delta_{ij}$. We will explore the properties of these states and see that it is easy to get expectancies using the density operator using this notation.

2.1.3 Density operator

Normally we describe the states of a quantum mechanical system as vectors in a Hilbert space: $|\Psi\rangle \in H$, observables are Hermitian operators on this space and the states evolve in time by unitary transformations. The state may equally well be expressed by an operator, called the density operator, defined as:

$$\hat{\rho} \equiv |\Psi\rangle\langle\Psi| \tag{2.1}$$

All information of the system carried in $|\Psi\rangle$ is also carried by its density operator counterpart $\hat{\rho}$.

In a given basis $\{e_i\}$ for the Hamiltonian describing the system, we can use the identity $\sum_i |e_i\rangle\langle e_i| = 1$ to write

$$\hat{\rho} = \sum_{i,j} |e_i\rangle\langle e_i|\rho|e_j\rangle\langle e_j| \tag{2.2}$$

We can interpret this as the density operator being represented by the density matrix with elements $\langle e_i|\hat{\rho}|e_j\rangle$. We shall not distinguish between the two representations and will use

both interchangeably.

If the system is in a mixed state, then the density operator take the form

$$\hat{\rho} = \sum_i p_i |\psi_i\rangle\langle\psi_i| \tag{2.3}$$

where the sum is over an ensemble, with p_i denoting the probability of the system being in the i'th state. The action of an operator $\hat{A}$ on the density matrix is given by $\hat{A}\hat{\rho}\hat{A}^\dagger$.

For a state $|\psi_i\rangle$ in an ensemble, the expectancy value of an operator $\hat{O}$ is given by $\langle\hat{O}\rangle_i = \langle\psi_i|\hat{O}|\psi_i\rangle$. For the statistical mixture this generalizes to

$$\langle\hat{O}\rangle = \sum_i p_i \langle\psi_i|\hat{O}|\psi_i\rangle \tag{2.4}$$

The trace of an operator $\hat{O}$ is defined as being the sum of the diagonal elements $\langle\phi_n|\hat{O}|\phi_n\rangle$. We see that

$$\mathrm{Tr}[\hat{\rho}\hat{O}] = \sum_i \langle\Psi_i|\hat{\rho}\hat{O}|\Psi_i\rangle = \sum_{i,j} p_j \langle\Psi_i|\Psi_j\rangle\langle\Psi_j|\hat{O}|\Psi_i\rangle = \langle\hat{O}\rangle \tag{2.5}$$

Multimode states

When two bases $|a_i\rangle$ and $|b_i\rangle$ are involved we may write the state of the system as

$$|\Psi\rangle = \sum_{i,j} c_{i,j} |a_i\rangle \otimes |b_j\rangle \tag{2.6}$$

yielding

$$\hat{\rho}_{AB} = |\Psi\rangle\langle\Psi| = \sum_{i,j,k,l} c_{i,j} c^*_{k,l} |a_i\rangle\langle a_k| \otimes |b_j\rangle\langle b_l| \tag{2.7}$$

the density operators of the subsystems can be found by making partial traces

$$\mathrm{Tr}_B[\hat{\rho}_{AB}] = \sum_n \langle b_n|\hat{\rho}|b_n\rangle = \hat{\rho}_A \tag{2.8}$$

and in a similar way for $\hat{\rho}_B = \mathrm{Tr}_A[\hat{\rho}]$. These operators are called reduced density operators. These can be used to get predictions of the subsystem in the same way as $\hat{\rho}$ can on the entire system. Whenever a quantum system consist of multiple parts, then we might find that these parts are correlated in a genuine nonclassical manor. It is this phenomenon that is called entanglement.

2.2 Entanglement

Entanglement is a physical phenomenon that enables us to do amazing things such as quantum cryptography, teleportation and demonstration of the nonlocality of quantum mechanics, to name a few. The formal definition of entanglement is as follows:

> Let $|\psi_{AB}\rangle$ denote the joint state of system A and B. Whenever this state cannot be written as a product of states of the subsystems $|\psi_{AB}\rangle \neq |\psi_A\rangle \otimes |\psi_B\rangle$, then the state $|\psi_{AB}\rangle$ is said that to be entangled or non-separable.

An unentangled state is called separable. A and B refer to two separate system.

In the rest of this section will we only consider bipartite system entanglement - entanglement between two and systems. Entanglement between any number of participating systems is possible but for the sake of keeping things simple, and relevant to this thesis, two participating systems will suffice.

Entanglement is a quantum correlation phenomenon, but it is not strictly correct to say that subsystems A and B are uncorrelated if $|\psi_{AB}\rangle$ is separable (unentangled); take for example the separable spin state

$$|\psi_{AB}\rangle = |\uparrow_A\rangle|\uparrow_B\rangle, \tag{2.9}$$

here the spins surely are correlated, as they both point in the same direction. But as seen by the definition of entanglement this is not an entangled state, the point being that correlations and entanglement is not the same thing.

The correlations between A and B in an entangled state are greater than what we could get from a separable state. We will give an example involving spin states below. An important property of entanglement is that it cannot be created locally[1], while classical correlations can. The only way to entangle system A and B is to have them interact with one another.

Later in this thesis we will encounter states similar to the spin-1/2 maximally entangled states that we will introduce below, these will serve as an example of entanglement. The states are defined in the a bipartite spin basis, the Hilbert space of each system is spanned by $|\uparrow\rangle$ and $|\downarrow\rangle$. The four maximally entangled states have the form:

$$\begin{aligned} |\phi^+\rangle &= \frac{|\downarrow\downarrow\rangle_{AB,z} + |\uparrow\uparrow\rangle_{AB,z}}{\sqrt{2}} & |\phi^-\rangle &= \frac{|\downarrow\downarrow\rangle_{AB,z} - |\uparrow\uparrow\rangle_{AB,z}}{\sqrt{2}} \\ |\psi^+\rangle &= \frac{|\downarrow\uparrow\rangle_{AB,z} + |\uparrow\downarrow\rangle_{AB,z}}{\sqrt{2}} & |\psi^-\rangle &= \frac{|\downarrow\uparrow\rangle_{AB,z} - |\uparrow\downarrow\rangle_{AB,z}}{\sqrt{2}} \end{aligned} \tag{2.10}$$

[1] Locally meaning that Alice and Bob sits in each their room, talking over a phone (or a similar communication device) agreeing on a way to prepare their part of the joint state and manipulate their part accordingly.

The *z* index denotes that the spin is along the *z*-direction. We will choose one of these states, say $|\psi^+\rangle$, to serve as our example.

Suppose we want to make a projective measurement of system A's spinstate onto the *z* basis. When we make such a measurement we collapse the state to either $|\downarrow\uparrow\rangle_{AB,z}$ or $|\uparrow\downarrow\rangle_{AB,z}$, each occurring with a probability of $\frac{1}{2}$. The point being that there is a correlation between the spin state of A and B, so if Alice were to measure $|\uparrow_A\rangle$ then Bob would measure $|\downarrow_B\rangle$ with a absolute certainty.

It seems like there is nothing un-classical about this kind of correlation. One might ask oneself how the above correlations are different from taking a red ball and a blue ball putting them in each their box, having a guy juggle with the boxes and then finally send them off to two observers Alice and Bob. Then Alice would surely know that Bob received a blue ball if she got a red, and so fourth. The argument for why this state contains more than classical correlations is not simple, but goes roughly as follows.

Alice and Bob would also find that their measurements were correlated if they where to measure about a different axis, even though a spin pointing in the positive *z*-direction is a balanced superposition of spin up and down along a different orthogonal axis. The spooky thing is that this remains true even though the two systems are spatially separated[2].

Alice and Bob can measure their spin state on each of the three axis (x,y,z). They do not have to agree upon their choice of axis in advance. When looking at the correlations of such measurement, one finds that the correlations exceeds what is classically permissible. Mathematically this is expressed by the Bell inequality which is to be discussed later in this thesis. This topic is much discussed through the years by famous physicists, but for now it is just important to know that the correlations are truly non-classical. For a great presentation of the problem of non-locality and entanglement see [15, Bertlmann's socks and the nature of reality].

2.2.1 Measure of entanglement

A bipartite system $|\psi_{AB}\rangle$ is called separable or not entangle if it can be decomposed into a direct product of pure states in the respective Hilbert spaces. In this case the reduced density matrix $\hat{\rho}_A = |\psi_A\rangle\langle\psi_A|$ and $\hat{\rho}_B = |\psi_B\rangle\langle\psi_B|$ are pure states. We know that

$$\mathrm{Tr}[\hat{\rho}^2] = 1 \tag{2.11}$$

for a pure state, so this is a good and easy way to determine if a system is not entangled. It is however more difficult to measure the level of entanglement in a system. In the

[2]The word "spooky" is due to Einstein, who did not like these actions at a distance. [1]

literature, there is no commonly agreed upon measure of entanglement.

This thesis takes off from a proposal for a loopholefree test of quantum non-locality [8], in this article they wish to break Bell's inequality $S_{Bell} \leq 2$. For the purpose of comparing the results in this thesis to the aforementioned articke, we will also use what we call the Bell parameter, S_{Bell}, as our measure of entanglement.

This measure might not be optimal for measuring the effect of our purification protocol, but it could reveal a true quantum purification feature if we are able to take a state with Bell parameter smaller than 2 to a state with Bell-parameter greater than 2.

There are another way to measure the entanglement namely the Von Neumann entropy [16, 17], which is often used when determining entanglement in a bipartite system. Another measure that is very usefull when one tries to drive a state towards a maximally entangled state, is to simple calculate the overlab between the two states, this measure has a maximum value of one. We choose howewer to use the ability to break Bell's inequality as the measure of entanglement in this thesis.

2.3 Bell's inequality

Bell's inequality offers a way to test very fundamental questions in quantum mechanics. It forces one to realize that quantum mechanics cannot coexist alongside a concept of locality. Bell's inequality offers these possibilities, but despite these very philosophical concepts it can be explained in very general terms not referring to quantum mechanics at all.

We will look at the probability

$$P(A, B|a, b), \tag{2.12}$$

defined as the probability of results A and B given the setting a and b. We do not have to think about quantum mechanics and measurements here.

We assumme that the results are dependant, so that we cannot factorize the probability function

$$P(A, B|a, b) \neq P_1(A|a)P_2(B|b) \tag{2.13}$$

If we assume that an hidden variable λ is present so that the factorization is possible, then we can write

$$P(A, B|a, b, \lambda) = P_1(A|a, \lambda)P_2(B|b, \lambda) \tag{2.14}$$

Here we have introduced our assumption of a hidden variable λ. The idea is that we imagine that there exists an underlying theory, knowledge of this theory enables us to predict

the outcome of measurements. We can obtain the original probability by integrating over a probability distribution $f(\lambda)$

$$P(A,B|a,b) = \int d\lambda f(\lambda) P(A,B|a,b,\lambda) \tag{2.15}$$

The two equations presented above both carry the assumption that such a hidden variable exist.

The purpose of Bell's theorem is to take this equation and put it in a form where it can be tested directly. In order to do this we look at a simple setup where the results A and B can only take the values 1 or -1. We introduce the parameter $E(a,b)$ given by

$$E(a,b) = P(1,1|a,b) + P(-1,-1|a,b) - P(1,-1|a,b) - P(-1,1|a,b). \tag{2.16}$$

We reproduce the work of Clauser-Holt-Shimony-Horne (CHSH) [18] using equations (2.15), (2.16) and some simple algebra and find that

$$E(a,b) = \int d\lambda f(\lambda) \bar{A}(a,\lambda) \bar{B}(b,\lambda) \tag{2.17}$$

where $\bar{A}(a,\lambda) = P_1(1|a,\lambda) - P_1(0|a,\lambda)$ and $\bar{B}(b,\lambda) = P_2(1|b,\lambda) - P_2(0|b,\lambda)$. Remembering that we are dealing with probabilities[3] we see that $|\bar{A}(a,\lambda)| \leq 1$ and $|\bar{B}(b,\lambda)| \leq 1$. We see that we can get

$$E(a,b) \pm E(a,b') \leq \int d\lambda f(\lambda) \bar{A}(a,\lambda)[\bar{B}(b,\lambda) \pm \bar{B}(b',\lambda)] \tag{2.18}$$

Looking at the absolute value of this equation we can get

$$\begin{aligned} |E(a,b) + E(a,b')| &\leq \int d\lambda f(\lambda) |\bar{B}(b,\lambda) + \bar{B}(b',\lambda)| \\ |E(a',b) - E(a',b')| &\leq \int d\lambda f(\lambda) |\bar{B}(b,\lambda) - \bar{B}(b',\lambda)|. \end{aligned} \tag{2.19}$$

Since $|\bar{B}(b,\lambda)| \leq 1$ we can get $|\bar{B}(b,\lambda) + \bar{B}(b',\lambda)| + |\bar{B}(b,\lambda) - \bar{B}(b',\lambda)| \leq 2$ using this property and the fact that $\int d\lambda f(\lambda) = 1$, we arrive at

$$|E(a,b) + E(a,b') + E(a',b) - E(a',b')| \leq 2 \tag{2.20}$$

This particular form of Bell's inequality is due to Clauser, Holt, Shimony and Horne (CHSH) [18]. The inequality is expressed in a very general way, it is mathematical

[3] If P is a probability then we know that P is positive and not greater than one.

identity and the involved probabilities could refere to many things other than quantum mechanics.

Bell's inequality is true whenever a hidden variable is assumed. Local realism is seen to be in conflict with quantum mechanics, so Einstein argued that this must exist a hidden variable that could explain this inconsistency. Bell's inequality can put this to the test, it is possible to perform a set of measurements and if we find Bell's inequality broken for these measurements then no hidden variable is present.

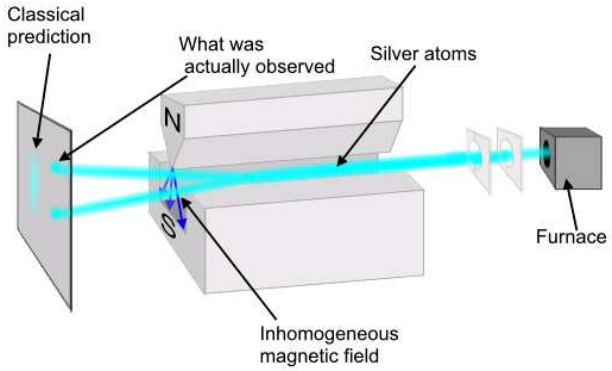

Figure 2.1: *The Stern-Gerlach experiment consists of deflecting a beam of Silver atoms in a inhomogeneous magnetic field. The result is surprising, as one finds that each silver atom been deflected to a fixed angle either upwards or downwards, not over an continuum of angles. The picture of an stern-gerlach experiment was found at www.wikipedia.org*

Bell's inequality enables us to test whether Einstein is right or if quantum mechanics is an non-(local realistic) theory.

Take for example an Stern-Gerlach experiment where the spin-$\frac{1}{2}$ particles are deflected either up or down along a chosen axis, this corresponds to the requirement that A and B in $P(A, B|a, b)$ is assumed to only take two values, here denoted -1 and 1. The conditioning on a and b is done by letting a and b denote different axis to measure the spin about.

When testing Bell's inequality on a Stern-Gerlach experiment we find that the Bell's inequality is broken. This forces us to discard the notion of a hidden variable in the Stern-Gerlach setup, and at a broader view, in quantum mechanics. We are thus forced to take back our notion of local-realism and accept that quantum mechanics is a non-local theory.

Bell's inequality was firstly put to an experimental test by A. Aspect [4] and many others since, all confirms that a quantum mechanical system can break Bell's inequality. Everytime this feed is achieved we prove that our world is non-local.

2.4 Continuous variable photonic states

In this section we will give an introduction to continuous variable photonic states. First their connection to creation and annihilation operators and then its description in quadrature phases and lastly we will give a description of squeezed states.

2.4.1 States of light

Maxwell's equations (2.21) which are rigorously explained in the literature [19, 20] describs the behavior of the electromagnetic phenomena, they stand as a beautiful unification of two fields that once were sought to have no common ground. Maxwell laid the foundation of modern field theory with these equations yielding a detailed account of light as electromagnetic waves.

$$\nabla \times \mathbf{H} = \frac{\delta \mathbf{D}}{\delta t}, \quad \nabla \times \mathbf{E} = -\frac{\delta \mathbf{E}}{\delta t}, \quad \nabla \cdot \mathbf{B} = 0, \quad \nabla \cdot \mathbf{D} = 0. \tag{2.21}$$

At this point in time[4] physics seemed triumphant with only "minor" worries about the nature of black-body radiation and of the photoelectric effect.

The investigation of these effects led to the quantum revolution. Planck had theorized that thermal radiation of light only happened in distinct and discrete quanta in order to make the spectra fit observations. Einstein took the idea further by ascribing the discrete nature to light itself and not just the radiation process, and used it to explain the photoelectric effect. Dirac addressed the issue of describing the quantized light fields interaction with a atom. He did this by associating to each mode of the light field a harmonic oscillator.

2.4.2 Photon creation and annihilation operators

The following derivations are completely analogous to the derivations for a quantum mechanical harmonic oscillator. A QM-oscillator have a set of energy levels and some operators to go up and down the energy ladder. In the case of photonic-states the levels are represented by the state containing a given number of photons. The operators that go up and down the energy ladder are photon creation and annihilation operators.

Let us introduce the creation and annihilation operators for a single mode field, $\hat{a}^\dagger$ and $\hat{a}$ respectively. Let $|n\rangle$ be the energy eigenstate corresponding to the Hamiltonian and energy given by,

$$\hat{\mathbf{H}}|n\rangle = \hbar\nu(\hat{a}^\dagger\hat{a} + \frac{1}{2})|n\rangle = E_n|n\rangle. \tag{2.22}$$

[4] In the start of the twentieth century.

Where the operators $\hat{a}$ and $\hat{a}^\dagger$ satisfy the following equation,

$$[\hat{a}, \hat{a}^\dagger] = 1. \tag{2.23}$$

Using this we can calculate the energy of the new state $\hat{a}^\dagger|n\rangle$, by applying $\hat{a}^\dagger$ from the left on (2.22), and using the commutation relation given above.

$$\hat{a}^\dagger \hat{\mathbf{H}}|n\rangle = E_n \hat{a}^\dagger|n\rangle = \hbar\nu\hat{a}^\dagger(\hat{a}^\dagger\hat{a} + \frac{1}{2})|n\rangle = (\hat{\mathbf{H}} - \hbar\nu)\hat{a}^\dagger|n\rangle \tag{2.24}$$

Comparing the first and last of these equations give $\hat{\mathbf{H}}\hat{a}^\dagger|n\rangle = (E_n + \hbar\nu)\hat{a}^\dagger|n\rangle$ in a similar way we get the equation $\hat{\mathbf{H}}\hat{a}|n\rangle = (E_n - \hbar\nu)\hat{a}|n\rangle$. These equations prove that $\hat{a}$ and $\hat{a}^\dagger$, respectively lower and raise the energy of the system. The operator $\hat{a}^\dagger\hat{a}$ has a special significance as its is called the number operator denoted $\hat{n}$, the effect of $\hat{n}$ on a number state is given by $\hat{n}|n\rangle = n|n\rangle$, the energy of these states are given by $E_n = \hbar\nu(n + \frac{1}{2})$. The effect of the creation and destruction operators is $\hat{a}|n\rangle = c_n|n-1\rangle$. Looking at the expression

$$\begin{aligned} (\langle n|\hat{a}^\dagger)(\hat{a}|n\rangle) &= \langle n|\hat{a}^\dagger\hat{a}|n\rangle = n \\ &= \langle n-1|c_n^* c_n|n-1\rangle = |c_n|^2 \end{aligned} \tag{2.25}$$

we easily get $c_n = \sqrt{n}$ and the same calculation for $\hat{a}^\dagger$ give us

$$\hat{a}|n\rangle = \sqrt{n}|n-1\rangle \qquad \hat{a}^\dagger|n\rangle = \sqrt{n+1}|n+1\rangle. \tag{2.26}$$

This property is the reason for the names, annihilation and creation operators. We can now see that an arbitrary number state can be manufactured by successive application of the creation operator $\hat{a}^\dagger$,

$$|n\rangle = \frac{(\hat{a}^\dagger)^n}{\sqrt{n!}}|0\rangle. \tag{2.27}$$

The number states form a complete basis and the states of different numbers are orthogonal. The shown properties of the number states make it a basis that is very easy to work with when doing many sorts of calculations, it is however not so easy to do experiments using number states.

From elementary quantum mechanics is it well known that the ground level of an harmonic oscillator does not have zero energy. This also apply to the description of light, the vacuum state $|0\rangle$ is more than just zero photons.

2.4.3 Coherent state of light

The number states as presented above have a uniform phase distribution, that is, there are no well defined phase for these states. Producing a number state for a large n does not result in a classical state of light. The number states for a large n does not have a well defined phase, and this is incompatible with what we see in classical light states.

The coherent states that we are about to introduce do have a nice classical limit, this makes them the states of choice when doing lab work and theory, at least in the case of this thesis.

The coherent states are given as the solution to the eigenvalue problem

$$\hat{a}|\alpha\rangle = \alpha|\alpha\rangle. \tag{2.28}$$

The above equation (2.28) defines the "right" eigenstates $|\alpha\rangle$ where as the "left" eigenstates are defined by $\langle\alpha|\hat{a}^\dagger = \alpha^*\langle\alpha|$. To find these states we utilize that the number states form a complete set. We can expand $|\alpha\rangle$ on these

$$|\alpha\rangle = \sum_{n=0}^{\infty} C_n|n\rangle. \tag{2.29}$$

Letting $\hat{a}$ act on this state yields

$$\hat{a}|\alpha\rangle = \sum_{n=1}^{\infty} C_n\sqrt{n}|n-1\rangle = \alpha\sum_{n=0}^{\infty} C_n|n\rangle, \tag{2.30}$$

comparing the coefficients of $|n\rangle$ in the last equation gives $C_n\sqrt{n} = \alpha C_{n-1}$ which will get us:

$$C_n = \frac{\alpha}{\sqrt{n}}C_{n-1} = \frac{\alpha^2}{\sqrt{n(n-1)}}C_{n-2} = \ldots = \frac{\alpha^n}{\sqrt{n!}}C_0. \tag{2.31}$$

Normalizing $|\alpha\rangle$ we find $C_0 = \exp(-\frac{1}{2}|\alpha^2|)$ and thus the state defined by (2.28) can be written as

$$|\alpha\rangle = \exp(-\frac{1}{2}|\alpha^2|)\sum_{n=0}^{\infty}\frac{\alpha^n}{\sqrt{n!}}|n\rangle, \tag{2.32}$$

we see that for every $\alpha \in \mathbf{C}$ there is a state $|\alpha\rangle$. In the literature [10, 11, 12] it can be found that the set of all coherent states form an over-complete basis that is not orthogonal.

The displacement operator $\hat{D}(\alpha)$ has the property that it can be used to generate coherent states from vacuum $\hat{D}(\alpha)|0\rangle = |\alpha\rangle$, it is defined as

$$\hat{D}(\alpha) = \exp(\alpha\hat{a}^\dagger - \alpha^*\hat{a}). \tag{2.33}$$

We are in particular interested in determining the physical meaning of α. First off we find the expectation value of photon number operator $\hat{n} = \hat{a}^\dagger \hat{a}$,

$$\langle \alpha | \hat{n} | \alpha \rangle = |\alpha|^2 \tag{2.34}$$

and in a similar way we can find $\langle \hat{n}^2 \rangle$ to be

$$\begin{aligned} \langle \alpha | \hat{n}^2 | \alpha \rangle &= \langle \alpha | \hat{a}^\dagger \hat{a} \hat{a}^\dagger \hat{a} | \alpha \rangle \\ &= \langle \alpha | \hat{a}^\dagger \hat{a}^\dagger \hat{a} \hat{a} + \hat{a}^\dagger \hat{a} | \alpha \rangle \\ &= |\alpha|^4 + |\alpha|^2 = \langle n \rangle^2 + \langle n \rangle \end{aligned} \tag{2.35}$$

This distribution has $\triangle n = \sqrt{\langle \hat{n}^2 \rangle - \langle \hat{n} \rangle^2} = \sqrt{\langle n \rangle}$ which give a Poisson distribution of the photon number. One can also find the distribution of phases for a coherent state which for a large $|\alpha|$ is given by a Gaussian distribution. Important properties of coherent states are that for large photon numbers they are well localized in phase. The coherent state resembles a classical state in many ways all though it really is a quantum state.

Most importantly is the fact that coherent states have all the properties of light produced by a LASER and as such they are very important in doing theory, as they describe closely the photonic-states used in the laboratories.

2.4.4 Quadrature operators

Working with complicated light-states, such as coherent states, one needs a way to characterize the properties of the state. The quadrature operator representation offers a way of representing many different light states. They are also easy to measure experimentally through the process of balanced homodyne measurement, we will give an introduction to balanced homodyne detection in section 2.5,

The quadrature operators are an photonic analog to the quantum momentum and position operators for light states but they are scaled so that they are dimensionless [11]. They are given by[5]

$$\hat{X} = \frac{1}{\sqrt{2}}(\hat{a}^\dagger + \hat{a}), \qquad \hat{P} = \frac{i}{\sqrt{2}}(\hat{a}^\dagger - \hat{a}). \tag{2.36}$$

They satisfy the commutation relation

$$[\hat{X}, \hat{P}] = \frac{i}{2}[(\hat{a}^\dagger + \hat{a}), (\hat{a}^\dagger - \hat{a})] = \frac{i}{2}([\hat{a}, \hat{a}^\dagger] - [\hat{a}^\dagger, \hat{a}]) = i \tag{2.37}$$

[5] A quadrature operator for any angle θ can be defined as $2^{-1/2}(\hat{a}\exp[-i\theta] + \hat{a}^\dagger \exp[i\theta])$. $\hat{X}$ and $\hat{P}$ as we use them are special cases given for $\theta = 0$ and $\theta = \pi/2$.

It is well known that we quantum mechanically cannot measure both position and momentum at the same time. It is nevertheless possible to present photonic-states in the $\hat{X}, \hat{P}$-phasespace, resulting in an easy graphical representation of different states.

A coherent state $|\alpha\rangle$ minimizes the uncertainties on the quadrature operators and it can be shown that the uncertainties in the X and P quadratures are equal [10, 11, 12]. The expectation values of the quadrature operators are easily found from their definition to be $\langle\hat{X}\rangle = \frac{1}{\sqrt{2}}(\alpha + \alpha^*) = \sqrt{2}\mathbf{Re}[\alpha]$ and $\langle\hat{P}\rangle = \frac{i}{\sqrt{2}}(\alpha^* - \alpha) = \sqrt{2}\mathbf{Im}[\alpha]$.

A plot of a coherent state in the $\hat{X}, \hat{P}$-phasespace is simply a circle of fixed minimal uncertainty radius, its center is situated at an phase angle θ away from the $\hat{X}$-axis at a distance $|\alpha|$ from the origo.

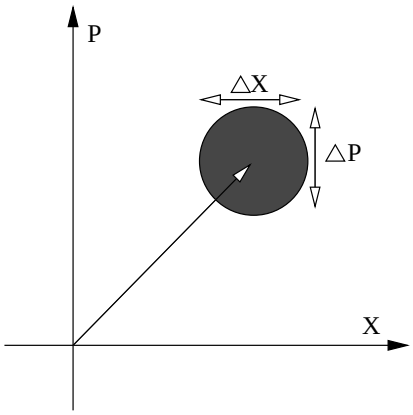

Figure 2.2: *Representation of a coherent state $|\alpha\rangle$ where the circle depicts the uncertainties. The uncertaincy, and with it the diameter in the plot, is independent of α. For a large photon number the relative uncertaincies become small.*

We know that the uncertainties in the quadratures for a coherent state are minimal and equal, but there exist a way to produce states where one the uncertainty in one quadrature is smaller than the minimal uncertainty, this process is called quadrature squeezing.

2.4.5 Quadrature squeezing

If two hermitian operators $\hat{A}$ and $\hat{B}$ satisfy the commutation relation $[\hat{A}, \hat{B}] = i\hat{C}$ then we know that according to Heisenberg's uncertainty relation the product of the uncertainties fulfills $\triangle\hat{A}\triangle\hat{B} \geq \frac{1}{2}|\langle\hat{C}\rangle|$ [14]. A state is squeezed if either

$$(\triangle\hat{A})^2 < \frac{1}{2}|\langle\hat{C}\rangle| \qquad \text{or} \qquad (\triangle\hat{B})^2 < \frac{1}{2}|\langle\hat{C}\rangle| \tag{2.38}$$

is true. It is obvious from Heisenberg that we cannot have both inequalities fulfilled, so when one operators expectancy is lowered the others must go up. The coherent states are

minimum uncertainty states with the same uncertainty as the vacuum, so when squeezing one of the quadrature phases we obtain a sub-vacuum level of noise in this quadrature.

We can define a squeezing operator

$$\hat{S}(\xi) = \exp[\frac{1}{2}(\xi^* \hat{a}^2 - \xi \hat{a}^{\dagger 2})], \tag{2.39}$$

which takes $\xi = s\exp(i\theta)$ as argument. Here s is the squeezing parameter and θ defines the axis on which to apply the squeezing. Later in this thesis we will encounter two mode squeezed states where we will use a different parameter for the squeezing namely $\lambda = \tanh(s)$, with $\lambda \in [0, 1]$.

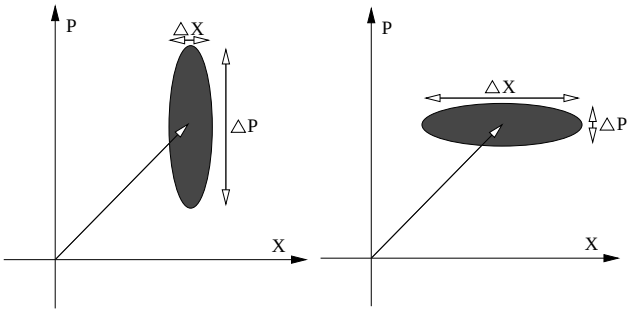

Figure 2.3: *Representation of a squeezed coherent state $\hat{S}(\xi)|\alpha\rangle$ for two different squeezing directions. Firstly the state is squeezed along the $\hat{X}$-axis and secondly along the $\hat{P}$-axis. The area of the ellipsis depicts the uncertainties.*

In this thesis we will only use $\theta = 0$, the effect of θ is illustrated above in figure 2.3. Later in this thesis we will apply phases to the squeezed state we are examining, this is found to be the same as squeezing along a different axis.

2.4.6 Multi mode representation

Until now, we have only dealt with single modes of light, this will not suffice for the scope of this thesis. We will often times need many modes of light to describe the entire system. We index the different modes by k and to each mode we have a set of annihilation and creation operators $\hat{a}_k$ and $\hat{a}_k^\dagger$. The state space of the multi mode system is spanned by the tensor product of number states $|n_k\rangle$,

$$|n_1 \dots n_N\rangle = \bigotimes_{k=1}^{N} |n_k\rangle_k = \frac{1}{\sqrt{n_1! \dots n_N!}} (\hat{a}_1^\dagger)^{n_1} \dots (\hat{a}_N^\dagger)^{n_N} |\mathbf{vac}\rangle \tag{2.40}$$

where $|\mathbf{vac}\rangle$ denotes the joint vacuum state of all N modes. The operators from mode k only acts on the state in mode k, giving a new commutation relation,

$$[\hat{a}_j, \hat{a}_k^\dagger] = \delta_{jk} \tag{2.41}$$

The displacement operator for a multimode field is simply the product of single mode operators, so

$$\hat{D}(\alpha_A, \beta_B)|0_A, 0_B\rangle = \hat{D}(\alpha_A)\hat{D}(\beta_B)|0_A, 0_B\rangle = |\alpha_A, \beta_B\rangle \tag{2.42}$$

The squeezing operator for multimode fields is more complicated than that, but we will only need to use the operator for two modes. The two mode squeezing operator takes the form,

$$\hat{S}_{jk}(\xi) = \exp[\xi^* \hat{a}_j \hat{a}_k - \xi \hat{a}_j^\dagger \hat{a}_k^\dagger] \tag{2.43}$$

where $\xi = s\exp[i\theta]$. As one can see from the form of this operator the two mode squeezing operator creates and annihilates pairs of photons. Applying $\hat{S}_{jk}(\xi)$ to the vacuum state following [10], we get

$$|\hat{S}_{jk}(\xi)\rangle = \mathrm{sech}(s) \sum_{n=0}^{\infty} [-\exp(i\theta)\tanh(s)]^n |n, n\rangle_{j,k} \tag{2.44}$$

Assuming $\theta = 0$ this can be rewritten using the squeezing parameter used later in this thesis $\lambda = \tanh(s)$ to

$$|\hat{S}_{jk}(\xi)\rangle = \sqrt{1-\lambda^2} \sum_{n=0}^{\infty} (-1)^n \lambda^n |n, n\rangle_{j,k}. \tag{2.45}$$

We see that the resulting state is entangled, this is due to the fact that any measurement of n_j and n_k on this state will be correlated.

2.5 Balanced homodyne measurement

The properties we will seek in the setup of this thesis can be found using a technique called balanced homodyne measurement. Balanced homodyne measurement can be used to obtain the quadrature phases for the different modes of light. Balanced homodyne detection does this in the following way.

One mode contains the signal we wish to measure, this mode has a annihilation operator $\hat{a}$. The mode in question is then mixed on a balanced beamsplitter with a mode

containing high intensity coherent state with annihilation operator $\hat{b}$, see figure 2.4.

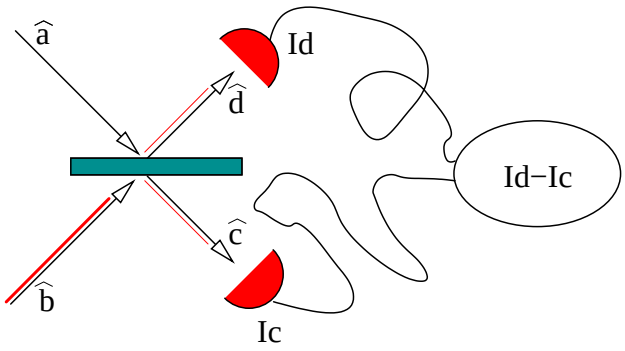

Figure 2.4: *Graphical presentation of balanced homodyne detection. We see the two incoming modes are mixed and the outgoing intensities are measured. The difference of the intensities are proportional to the quadrature phase of the incoming mode that we want to measure, $\hat{a}$.*

The balanced beamsplitter gives the following relation between the operators of the incoming and outgoing modes, [10, 11, 12]

$$\hat{c} = \frac{\hat{a} + i\hat{b}}{\sqrt{2}} \qquad \hat{d} = \frac{\hat{b} + i\hat{a}}{\sqrt{2}}. \tag{2.46}$$

It is easy to experimentally measure the intensity of the outgoing modes, this amounts to measuring the expectancy value of the number operator in the mode $I_c = \langle \hat{c}^\dagger \hat{c} \rangle$ and $I_d = \langle \hat{d}^\dagger \hat{d} \rangle$, this is done by measuring the classical current the intensity produces. When we subtract one intensity from the other we get the following expression, in terms of modes $\hat{a}$ and $\hat{b}$

$$I_c - I_d = \langle \hat{c}^\dagger \hat{c} - \hat{d}^\dagger \hat{d} \rangle = i\langle \hat{a}^\dagger \hat{b} - \hat{a}\hat{b}^\dagger \rangle \tag{2.47}$$

The mode belonging to $\hat{b}$ is in a coherent state with $\hat{n} \gg 1$, called $|\beta \exp[-i\omega t]\rangle$, here β is the complex number describing the coherent state and the exponential function gives the time evolution. We can represent β by its length and phase $\beta = |\beta| \exp[-i\psi]$, yielding

$$I_c - I_d = |\beta| \langle \hat{a} \exp[i\omega t] \exp[-i\theta] + \hat{a}^\dagger \exp[-i\omega t] \exp[i\theta] \rangle \tag{2.48}$$

where we have set $\theta = \psi + \pi$. The trick to homodyne detection is to mix the mode of light one want to measure, with a strong coherent field with the same frequency. The effect of this is a cancelling out of the frequencies of the mode of light one want to measure. Thus setting $\hat{a} = \hat{a}_0 \exp[-i\omega t]$ yields

$$I_c - I_d = \sqrt{2}|\beta| \langle \hat{X}(\theta) \rangle \tag{2.49}$$

with $\hat{X}(\theta) = \frac{\hat{a}_0 \exp[-i\theta] + \hat{a}_0^\dagger \exp[i\theta]}{\sqrt{2}}$. Setting θ equal to 0 and $\pi/2$ leaves us with the quadrature phases as we know them, $\hat{X}$ and $\hat{P}$ respectively.

The result is that we can measure any quadrature (we are free to choose θ) by measuring the difference between two classical currents. It is more accurate to say that what we measure is proportional two the quadratures, but after a calibration procedure we will be able to obtain the results equal to the actual quadratures.

2.6 Gaussian states

The Gassian function $f(x) = a \exp[-(x-b)^2/c^2]$ is the also referred to as the normal distribution. The reason for this is that it describes the limiting distribution of many naturally occurring phenomenons. We include this here because the distribution of the values of the quadrature phases in a coherent state is given as a Gaussian distribution. Gaussian distribution occurs both in vacuum, single mode and two mode states. These kind of states will be used to a large extent in this thesis.

2.7 Summary

In this chapter we have presented some of the basic formalisms that will be used throughout this thesis, namely density operators, bipartite systems, harmonic oscillator photon states, continuous variable states and quadrature operators.

We also introduced the important concept of entanglement along with Bell's inequality which offers a test of quantum non-locality and which will serve as our measure of entanglement in this thesis. Finally we presented a way to measure quadrature phase operators through the process of balanced homodyne detection.

For detailed knowledge of the concepts presented in this chapter, we will refer the reader to the articles and books cited throughout the chapter.

Chapter 3

Quantum information

The main concern of this chapter is to introduce the field of quantum information: the possibilities it offers and the problems it faces. We will focus on chosen results from the field which will exemplify the possibilities that quantum informations, quantum simulations and quantum computation presents.

We will also present a list of advantages and disadvantages to consider when comparing continuous variables to qubits. The list will focus on their properties related to quantum information, measurements and decoherence. And finally, we talk a bit on the differences between error-correcting and purification.

3.1 Introduction to the quantum information

The starting point for a study of quantum information is the realization that information is physical. This was realized in the 1980's by Landauer and Bennett, when trying to reconcile Maxwell's demon[1] with the second law of thermodynamics. They found that the demon must collect and store information about the incoming molecules.

This process cannot go on forever. Given the finite memory of the demon, information must eventually be erased, and at this point we finally bring balance to the energy equation.

If the demon were to be lazy and neglect the erasure, then we are forced to associate some entropy to the recorded information. The lesson learned is that there is a connection between the concept of information and physics; it is only natural to consider how

[1]Maxwell had envisioned a gas in a box, divided by partition into two parts A and B. This partition contains a shutter operated by a demon. The demon observes the molecules in the box as they approach the shutter, allowing the fast ones to go through from A to B and slow ones from B to A. Thus A cools and B is heats up, with a negligible work done, violating the second law of thermodynamics.

quantum mechanics fits into this picture.

The key difference between quantum information and classical information is the superposition principle. A classical bit, as we know them from the binary numbers in computers, is either **on** or **off**. We represent this by assigning to them the values 1 and 0, respectively.

Classical bits are used to carry information, which can be manipulated and read out without disturbing them.

The quantum mechanical equivalent to a classical bit is the "quantum bit" or qubit for short. A qubit is a state in a two-dimensional Hilbert space that take the form given by (3.1). Unlike a regular bit which can carry only the values either 0 or 1, the qubit also have the possibility to be in a superposition of 0 and 1.

$$|\psi\rangle = a|1\rangle + b|0\rangle, \qquad |a|^2 + |b|^2 = 1, \qquad \{a, b\} \in \mathbb{C}. \tag{3.1}$$

The qubit can thus be represented by a vector in a two-dimensional Hilbert space, using the same basis vectors $|0\rangle$ and $|1\rangle$ as in the classical case. We perform measurements on the qubits by making a projection onto this basis. The outcome of the measurements are probabilistic (and hence not deterministic as with classical bits) - we will obtain $|0\rangle$ with probability $|a|^2$ and $|1\rangle$ with probability $|b|^2$.

Making measurements change the system in a probabilistic manor in sharp contrast to the classical case, this may seem like an disadvantage over the classical bit, but it allows one to make calculations in a new, and often superior, way.

3.1.1 Quantum computation

Quantum computation is the field that deals with ways to calculate problems using qubits. Large books [16] are written on the subject, and the results are often amazing. The power of quantum computation can be seen in the procedure of Deutsch and Josza, the result of which is presented below.

Imagine a function $f(x)$ which could return either 0 or 1 depending on its argument $x = 0$ or $x = 1$. The job at hand is to figure out whether $f(1) = f(0)$ or $f(1) \neq f(0)$. Classically this job needs two calculations ($f(0)$ and $f(1)$), but when using qubits it can be done in one, this amazing result is described originally by Deutsch and Josza, and the detailed calculations can be found in [16, 21, 22].

There are many more examples of qubit-algorithms that perform calculation tasks faster than regular algorithms, one that is often mentioned is the ability to factor products of large primes. This is particularly important due to the fact that much cryptography

today rely on the fact that factorization of the product of two large unknown primes will take a time comparable to the age of the universe for a classical computer. This quantum computation protocol was due to Shor, who alongside Grover have made algorithms that significantly speed up many computation processes [16].

3.1.2 Quantum simulation

Another problem that is of tremendous interest to physicists is the problem of simulating quantum behavior. This idea was originally formed by Richard Feynman [23], in his paper from 1982. When looking at qubits and the way they behave, nothing has been shown that cannot be done on a regular computer simulating quantum behavior, so why not just do that?

The answer is that the amount of data contained in a qubit state is incredible large. A state consisting of N-qubits can be expressed as a vector in a 2^N-dimensional space. A general normalized vector can be expanded in the basis spanned by all combinations of $|0\rangle$ and $|1\rangle$ as,

$$|\psi\rangle = \sum_{x=0}^{2^N-1} a_x|x\rangle \tag{3.2}$$

where x is the binary number made up from the combination of zeros and ones. So to characterize an reasonable number of qubits, say $N = 100$, one needs $2^{100} \approx 10^{30}$ complex numbers a_x. No classical computer can handle this amount of data.

3.1.3 Physical qubit systems

We have found that a classical computer cannot simulate a quantum system, due to the huge amount of data involved. The not so surprising solution is to use physical quantum system to simulate the quantum behavior in a controlled manor.

There are many quantum systems that could fulfill the role of a qubit as described in (3.1). It is very natural to interpret (3.1) as the spin state of a object with spin-$\frac{1}{2}$. Here $|0\rangle = |\downarrow\rangle$ and $|1\rangle = |\uparrow\rangle$ could represent the spin along an particular axis, $\{x, y, z\}$. In this case the two complex numbers a, b from eqn. (3.1) describe the orientation of the spin in three dimensional space.

Another two-level system of importance is provided by a photon, which can have two independent polarizations. Either horizontally and vertically or clockwise and counter clockwise.

The key difficulty in realizing such systems is that one needs very strong coupling between the different qubits without a strong coupling to the environment. A strong

coupling to the environment would destroy the information carried by the qubits through the process of decoherence.

3.2 Decoherence and purification

3.2.1 Decoherence

Take the example of a bipartite state, one part of the state is sent off to Alice and the other part is send to Bob. A strong correlation in the quantum state is needed in order to make sure that Alice and Bob measure what they would expect from their entangled state. When Alice measure on particle A she will know with a high probability what Bob will measure on particle B.

This strong correlation is essential for quantum information processing. When one need to process the informations a strong interaction is needed, but this implies a great difficulty.

Isolation of systems that exhibit a strong interaction needs to be done to near perfection, in order to prevent it from interacting with other things than what wanted. A perfect isolation is obviously impossible, though highly desirable, so it is important to figure out and take into account, what this contact to the environment do to a system.

In general, interaction between states generates entanglement. When the states in question are in contact with the environment, entanglement is produced between the environment and the states. The result is that the state in consideration evolve away from the ideal quantum mechanical superposition state. The states evolve towards a statistical mixture of states, due to the entanglement to the environment. The result of this process is that we are losing the correlation we wished to utilize.

This process of decoherence is a major obstacle when transmitting quantum information over longer distances, as this makes for a longer time where the states are in contact with the environment.

We seek a way to regain the original entanglement through a socalled purification-process. There are many ways to purify a qubit state, in a later chapter we will go into one of these in some details, as this is this protocol we want to make a continuous version of. For now we just need to know that such protocols exists.

3.2.2 Purification

There exists a range of different methods for obtaining a state with a higher entanglement, these fall in different categories: purification, distillation and error correcting methods.

The names distillation and purification cover the same phenomenon.

Purification protocols work on a ensemble of identically prepared states and offer a method of error finding. When an error is detected then the infected state is removed from the ensemble.

Looking at a single state from the ensemble where an error has occurred, we find that the result of the protocol is obviously not that of entanglement purification/distillation, as the state is discarded. But on average the surviving states will be driven towards a purer and more concentrated state. This thesis will propose a method for purifying continuous variable states that already exhibits a high degree of entanglement.

It it important to think of the purification protocol as working on an ensemble of states. We can think of the fidelity - which is the average value of the overlap between the states in the ensemble and an optimal purified state - as an measurement of the effect of the purification protocol.

3.2.3 Error correcting

The concept of error-correcting codes is somewhat more complicated. Peter Shor constructed the first such code, which used three copies of the each classical bit in the qubit, [17].

$$a|1\rangle + b|0\rangle \rightarrow a|111\rangle + b|000\rangle \tag{3.3}$$

By applying a range of operations to this state it is possible to eliminate the error from the state without destroying it. This way of dealing with errors is superior to the purification protocols described above. The reason for the superiority is that it corrects error instead of throwing away infected states, and thus works on all states and not just on average. It is however also far more difficult to implement such a protocol, as there are many steps involved.

3.3 Continuous variable quantum information

Recently, much attention has been devoted to the investigation of continuous variable quantum systems used for quantum information processing. One of the reasons for this is that there exists a large toolbox for working with continuous variable systems.

It is especially easy to work with Gaussian states of light which includes: single and two mode squeezed coherent states. These states can be manipulated easily by a group of linear optical elements as well as through homodyne detection. An important point is that the tools are easy to employ for both theorists and the experimentalists. Also, Gaussian

states are very easy to characterize theoretically.

Amazing results have already been produced in the field of continuous variable quantum optics. Recently an experimental working setups performing continuous variable teleportation have been demonstrated at the The Niels Bohr Institute. This is just a single result in a huge field of research, a field that have seen tremendous interest in the last few decades.

In this and the previous chapters, qubit states have been used to familiarize the reader with the concept of entanglement. This choice of using qubits instead of continuous variable states was solely due to the easily comprehendable way the phenomenons can be presented using the qubit formalism.

This thesis deals with continuous variables, and not qubit states. The reason for using continuous variables are manifold, we will list a number of advantages below:

- Due to the weakly interacting nature of the photon, continuous variable optical systems are subjected to relative low decoherence rates in comparesion with for example atomic or solid state systems. It should be mentioned though that this property is not unique to continuous variable photonic states, we could state the same advantage for a qubit that is being represented by the polarization modes of a photon.

- Continuous variables can utilize the powerfull tools developed over the last 4 decades by experimental quantum optics: parametric downconversion in nonlinear crystals, femtosecond laser pulses, controlled atom-photon interaction or cavity QED techniques. We will not present details on these techniques in this thesis, it will suffice to know that highly developed tools for processing continuous variable state exists.

- The most important reason for using continuous variable light systems, is that continuous variable quantum information protocols behave deterministicly. Their discrete variable counterparts, qubits, are probabilistic.

  This is an huge advantage over the qubits, as we do not have to check whether a probabilistic protocol where successfully completed, but just employ the protocol and read out the results.

The major drawback on the other hand are much due to the same reasons as the last and most important advantage. When one encodes information into a qubit represented by a photon and sends it to a receiver. Then the receiver either receives the photon or not, and can then use error correcting codes to read the message send to him.

When transmitting continuous variable states the states are always partly lost due to decoherence and the receiver has to be more cautious in choosing whether he should believe in his measurements. This is the reason that a continuous variable purification protocol is of great importance, as such a protocol could solve this problem and thus leave continuous variable photon states superior to qubit states.

3.4 Summary

A brief introduction to quantum information has been given, including the promises it holds for quantum computing. A short presentation of the decoherence problem along with the solution that purification offers has also been presented.

We found that a purification protocol for continuous variables would be a remarkable tool when doing quantum information experiments. The existence of such a protocol would make deterministic continuous variables reliable as carriers of quantum information.

Chapter 4

Wigner Functions

The purpose of this chapter is to give an introduction to Wigner functions. In building and exploring the purification protocol that is the subject of this thesis, Wigner functions will be the tool of choice. Wigner functions are quasi-probability distributions which have a range of smart properties that we will take advantage of. These properties will be presented in this chapter along with the connection between Wigner functions and the concept of non-locality. Finally, the phase space representation of Wigner function for a Guassian state are presented, as this is the form of the Wigner function the calculations in this thesis will use the most.

A classical probability distribution, $P(x_1, \ldots, x_n)$, gives the probability of a certain outcome of the n variables. Classically you can talk about the probability of getting two sixes in a game of dice. But in quantum mechanics things are complicated by the the concept of non-commuting variables.

It is well known in quantum mechanics that it is impossible to measure both the position operator x and the momentum operator p, or any other set of non-commuting operators, at the same time. Therefore we cannot speak of the probability of having a particle at position x with momentum p, thus making the concept of a true probability distribution impossible.

There are nonetheless, functions that bear some resemblance to classical probability distributions. It is possible to extract averages and probability densities for one variable, from this group of functions. The Wigner function is one[1] of these. It was introduced by E.P. Wigner to study quantum corrections to classical statistical mechanics, but has since found use many places - one of which is of particular interest, namely in quantum optics.

[1]The are many other distributions, see for example [10]

4.1 The Wigner function

The Wigner function is defined for an arbitrary density operator $\hat{\rho}$ as [24]

$$W(q,p) \equiv \frac{1}{2\pi\hbar}\int dx \langle q+\frac{1}{2}x|\hat{\rho}|q-\frac{1}{2}x\rangle e^{ipx/\hbar} \tag{4.1}$$

where $|q \pm \frac{1}{2}x\rangle$ are eigenkets of the position operator. If the state in question is in a pure state, e.g. $\hat{\rho} = |\psi\rangle\langle\psi|$, then we find

$$W(q,p) = \frac{1}{2\pi\hbar}\int dx\ \psi^*(q-\frac{1}{2}x)\ \psi(q+\frac{1}{2}x)e^{ipx/\hbar} \tag{4.2}$$

where $\langle q+\frac{1}{2}|\psi\rangle = \psi(q+\frac{1}{2})$.

The following calculation demonstrate how we can calculate a probability function of a state, from the Wigner function. We demonstrate this in the case of a pure state, the generalization to a mixed state is straightforward [24]

$$\begin{aligned}\int dpW(p,q) &= \frac{1}{2\pi\hbar}\int dpdx\ \psi^*(q-\frac{1}{2}x)\ \psi(q+\frac{1}{2}x)\ e^{ipx/\hbar} \\ &= \int dx\ \psi^*(q-\frac{1}{2}x)\ \psi(q+\frac{1}{2}x)\ \delta(x) \\ &= |\psi(q)|^2,\end{aligned} \tag{4.3}$$

where q is the position operator. In a similar way we can calculate the probability density for the momentum p, but in order to do the integral $\int dq\ W(p,q) = |\varphi(p)|^2$ we need to include the Fourier transform $\varphi(p)$ of the position representation $\psi(q)$, see [24] for details. It is also possible to find the expectancy value of a operator by performing the integral

$$\langle\hat{A}\rangle = \mathrm{Tr}[\hat{\rho}\hat{A}] = \int dqdpA(p,q)W(p,q) \tag{4.4}$$

The lesson learned is that there exists an easy way to get usable information from a Wigner function.

4.2 Wigner function of a Gaussian states

The Wigner function of a Gaussian state in phase space takes a particular simple form. We will calculate Wigner functions of Gaussian states at a later point in this thesis and we will therefore use some time to present it now.

The Wigner function of a Gaussian state only depends on the first and second mo-

ments of the quadrature operators. The first moment $\langle r_k \rangle$ of r_k is defined as

$$\langle r_k \rangle = \langle \phi | r_k | \phi \rangle = \int dpdq \; r_k W(q,p) \tag{4.5}$$

and the second moment is defined for every combination of two r_k's as

$$\langle r_j r_k \rangle = \langle \phi | r_j r_k | \phi \rangle = \int dpdq \; r_j r_k W(q,p) \tag{4.6}$$

In the two equations above $|\phi\rangle$ was the wavefunction for the Gaussian state. The last two equalities simply uses what we found in 4.4.

The Wigner function of a Gaussian state is completely specified by the first and second moments of the quadrature operators r_k where $r = (x_1, p_1, \ldots, x_n, p_n)^T$. One can replace the quadrature operators with numbers when evaluating a state given by a Gaussian density operator [25], this is a property that will prove very useful later.

In the book by J. Perina [26], detailed calculations are presented that leads to the Wigner function of an n-mode Gaussian state. The calculations are somewhat long and complicated, and it would not serve a reasonable purpose to present them here.

Instead of referring to the density matrix as given in (4.1), we here refer to the Wignerfunction defined on phase space. J. Perina [26] finds that for a n-mode Gaussian state the Wigner function takes the form

$$W(r) = \frac{1}{\pi^n \sqrt{\det \gamma}} \exp[-(r-d)^T \gamma^{-1} (r-d)], \tag{4.7}$$

where d is the vector of first moments $d_j = \langle r_j \rangle$, and γ is the covariance matrix, with matrix elements given by

$$\gamma_{i,j} = \langle r_i r_j + r_j r_i \rangle - 2 d_i d_j. \tag{4.8}$$

4.2.1 Covariance matrices

For a n-mode vacuum state the covariance matrix is given as $\gamma_{vac} = I_{2n}$, where I_{2n} is the identity matrix of rank $2n$. This can be seen by calculating all the different elements of the matrix. The following calculations are done for the case $d_j = 0$, but it is easy to include a nonzero d as well. The reason for choosing $d_j = 0$, besides for simplicity, is that the different quantum states of light that we will encounter in this thesis, all have the this property.

When calculating the different elements in the covariance matrix for vacuum, we need

to look at the expectancy of $r_i r_j + r_j r_i$ in a vacuum state. In order to have a non-vanishing matrixelement we need an equal number of creation and annihilation operators in at least one of the terms. When the quadrature operators of i and j belongs to different modes, this can never be the case. For the quadrature operators of i and j belonging to the same mode, but representing $\hat{X}$ and $\hat{P}$ respectively, we get

$$\begin{aligned}
\gamma_{i,j} &= \langle 0|r_i r_j + r_j r_i|0\rangle \\
&= \langle 0|\frac{1}{\sqrt{2}}(\hat{a}^\dagger + \hat{a})\frac{i}{\sqrt{2}}(\hat{a}^\dagger - \hat{a}) + \frac{i}{\sqrt{2}}(\hat{a}^\dagger - \hat{a})\frac{1}{\sqrt{2}}(\hat{a}^\dagger + \hat{a})|0\rangle \\
&= \langle 0|\frac{i}{2}(\hat{a}^{\dagger 2} - \hat{a}^\dagger\hat{a} + \hat{a}\hat{a}^\dagger - \hat{a}^2 + \hat{a}^{\dagger 2} + \hat{a}^\dagger\hat{a} - \hat{a}\hat{a}^\dagger - \hat{a}^2)|0\rangle \\
&= 0
\end{aligned} \tag{4.9}$$

In a similar way we can calculate the expectancy for $i = j$ and get $\gamma_{i,i} = 1$. The result of all this is that the covariance matrix of a n-mode vacuum state is given as

$$\gamma_{i,j} = I_{2n} \tag{4.10}$$

The covariance matrix for a two mode squeezed state with $d_j = 0$ can be calculated in a similar way, and it is found to be given as, see [8]

$$\gamma_{TMS} = \begin{bmatrix} \cosh 2s & 0 & \sinh 2s & 0 \\ 0 & \cosh 2s & 0 & -\sinh 2s \\ \sinh 2s & 0 & \cosh 2s & 0 \\ 0 & -\sinh 2s & 0 & \cosh 2s \end{bmatrix} \tag{4.11}$$

where s is the squeezing parameter as introduced in the chapter on the theoretical background.

4.3 Properties of Wigner functions

One very important property of Wigner functions is, that they can take on negative values. This is not consistent with the definition of a classical probability distribution, thus one use the expression: quasi-probability distribution function.

The negativity of a Wignerfunction is a necessary but not sufficient condition for breaking Bell's inequality, the argument leading to this profound statement will be outlined below.

The Wigner function of a Gaussian state is, as can be found from the calculations done above, itself Gaussian and does therefore not give negative values.

$$W(\text{Gaussian}) \geq 0 \tag{4.12}$$

When the Wigner function of a state is always greater than or equal to zero then we may interpret the distribution function as a classical probability distribution. When this is the case then the Wigner function provides a fully working hidden variable theory, and we are thus unable to break Bell's inequality. It is therefore necessary to have a Wigner function that is not everywhere positive in order to break Bell's inequality.

This thesis will propose a way to purify states to a level where they break Bell's inequality, but we start our procedure with states that are all Gaussian and thus positive. All the normal unitary operations such as beamsplitters and phaseshifters are all Gaussian operators and leaves a Gaussian state Gaussian.

It has been proven many places that Gaussian entanglement distillation requires non-Gaussian operations, [27, 28, 29]. These non-Gaussian operations could come in the form of photon subtractions or homodyne measurements. As we will see later in this thesis we will use both photon subtraction and homodyne detection in order to generate and purify states capable of breaking Bell's inequality.

The fact that one needs a non-Gaussian state in order to break Bell's inequality is referred to as the "no-go"-theorem, it is impossible for a Gaussian state to break Bell's inequality.

4.3.1 Trace and Wignerfunctions

The mathematical identity presented in this section will prove to be of great help throughout this thesis. The Wigner function of an operator $\hat{A}$ which not necessarily is the density operator is defined as:

$$W_A(r) = (2\pi)^{-1} \int dx \, \langle q - x/2|\hat{A}|q + x/2\rangle \exp[ipx]. \tag{4.13}$$

The above definition is for one mode but it is easy to generalize to more.

We will show that the trace over N modes of the product of two operators $\hat{A}$ and $\hat{B}$ can be expressed as an integral over their Wigner functions

$$\text{Tr}[AB] = (2\pi)^N \int d^{2N} r W_A(r) W_B(r) \tag{4.14}$$

We will prove this for one mode $(N = 1)$. The general result follows in a similar, but

more space consuming way. Writing the righthand side of the above equation we find,

$$\begin{aligned} 2\pi \int dr W_A(r) W_B(r) &= (2\pi)^{-1} \int dq dp dx' dx'' \langle q - x'/2|\hat{A}|q + x'/2\rangle \exp[ipx'] \\ &\quad \times \langle q - x''/2|\hat{B}|q + x''/2\rangle \exp[ipx'']. \end{aligned}$$

Using the identity $\int dp \exp[ipx] = 2\pi\delta(x)$ we can calculate

$$\begin{aligned} 2\pi \int dr W_A(r) W_B(r) &= \int dq dx' dx'' \langle q - x'/2|\hat{A}|q + x'/2\rangle \delta(x' + x'') \\ &\quad \times \langle q - x''/2|\hat{B}|q + x''/2\rangle \\ &= \int dq dx' \langle q - x'/2|\hat{A}|q + x'/2\rangle \langle q + x'/2|\hat{B}|q - x'/2\rangle. \end{aligned}$$

Finally, making a change of variable $y' = q - x'/2$ and $y'' = q + x'/2$ we arrive at

$$\begin{aligned} 2\pi \int dr W_A(r) W_B(r) &= \int dy' dy'' \langle y'|\hat{A}|y''\rangle \langle y''|\hat{B}|y'\rangle \\ &= \int dy' \langle y'|\hat{A}\hat{B}|y'\rangle = \mathrm{Tr}[\hat{A}\hat{B}]. \end{aligned}$$

where we have used the identity $\int dx''|x''\rangle\langle x''| = 1$. This proves (4.14), for one mode.

This result is used in both cases where we do non-Gaussian operations in this thesis. Firstly when we do photon subtraction and secondly when we condition on a homodyne detection, we will elaborate on this latter in the thesis.

4.4 Summary

The Wigner function has been introduced as a quasi-probability distribution function, that has a range of nice properties when calculation expectancies and traces. They will be used throughout this thesis.

We also fund that there exists a “no-go” theorem for Gaussian states when it comes to breaking Bell’s inequality. It is however possible to break Bell’s inequality if we apply a proper non-Gaussian operator to the state in question, this will also be used later on in this thesis.

Chapter 5

Preparation of the system

This chapter will present a loophole[1] free setup for breaking Bell's inequality, following to a large extent the calculations done in [8] which was also done at an earlier time by H. Nha and H.J. Carmichael [30].

The setup presented by [8, 30] and in this chapter, for a loophole-free test of Bell's inequality, produces the quantum state that we will try to purify later. Knowledge of how this state came to be is thus important for the complete understanding of the purification protocol that will be presented in the next chapter. Here we will deal with the above mentioned state, and include a presentation of the nomenclature, theoretical and experimental concepts used throughout the remainder of this thesis.

In quantum information theory we deal with entanglement between two distant points in space: A and B. Historically two persons - Alice and Bob - have been agreed upon as the residents at these points in space, we will use (A, B) and (Alice, Bob) interchangeable.

5.0.1 Outline of the experiment

A source supplies two mode squeezed vacuum states, one mode is send towards Alice, the other towards Bob. Each mode impinge on a unbalanced beamsplitter with high transmittance, and the reflected part of the state is subjected to a photo-detector. If the photo-detector goes "click" then we have subtracted a photon from the mode of light. When both detectors goes click we use the state in our Bell statistic.

After the subtraction of photons we measure the outcoming quadratures using highly efficient homodyne detectors. It is possible to use these measurements to produce the

[1] In a dictionary the following is said, defining a loophole:- *a means of escape or evasion; a means or opportunity of evading a rule, law, etc.: There are a number of loopholes in the tax laws whereby corporations can save money.*

joint probability distributions, and from this the correlation coefficients that leads to the violation of Bell's inequality.

5.1 Motivation

Einstein, Podolsky and Rosen (EPR) advocated in their paper from 1935 [1], that if local realism is taken for granted, then quantum theory is an incomplete description of the physical world. John Bell's inequalities made it possible to put this question, the question of quantum mechanics versus locality, to an experimental test.

The urge to break Bell's inequality experimentally have been great among physicist in the last decades. One of the pioneers was A. Aspect [4] who did an experiment where he measured on the correlations between the polarizations on photonic states in the abstract he writes:"*The results are in good agreement with quantum mechanical predictions but violate Bell's inequalities by 5 standard deviations.*"

Many experiments have since been constructed that lead to violation of the aforementioned inequality. They have all of them, including the experiment of A. Aspect, suffered from loopholes, either locality loopholes or detector efficiency loopholes.

5.1.1 Locality and detector efficiency loopholes

A test of Bell inequality typically involves two distant parties Alice and Bob, who simultaneously measure on their part of the shared quantum system.

Both parties randomly choose between measuring one of two properties a_1 or a_2 (b_1 or b_2). To avoid the locality loophole[2] these events have to be spacelike separated so that no signal can travel from one to the other. The speed of light is the fastest a signal can travel, so this suggests that optical systems are very well suited when one want to avoid the locality loophole.

The detector efficiency loophole occurs when the detection apparatus has an low efficiency. A low detection efficiency makes it possible to explain the observed correlations solely on the grounds of a low efficiency, and thus not due to the quantum phenomenon causing the correlations.

The experimental setup that will be presented in this chapter, uses continuous variable light states and high efficiency homodyne detection, thus discarding the locality and the detector efficiency loophole.

[2]The experimental data admit a local realistic description if communication between the parties is possible.

5.1.2 Degaussification

In order to break the inequality we need to construct a non-Gaussian state that has a Wigner function that is not positive definite. The reason for this is given by the "no-go" theorem for Gaussian states that we touched upon earlier.

We perform the de-gaussification step by subtracting a photon from each mode on a two mode coherent squeezed vacuum state. The subtraction is done by reflecting a small part of each mode onto a single photon detector. The photo-detectors do not have to have a very high detection efficiency as they only serve to conditionally prepare the state. We only use the states where both detectors went "click", in our Bell inequality statistic, and the setup is therefore not subject to the detector efficiency loophole.

5.2 Conceptual model of the conditional prepared state

The conceptual scheme of the setup is depicted in figure 5.1. A source generates a two mode squeezed vacuum state[3] in the modes A and B. A squeezed vacuum state has the expectancy value for both quadrature operators equal to zero, and a mean photon number that grows with the amount of squeezing applied to the state.

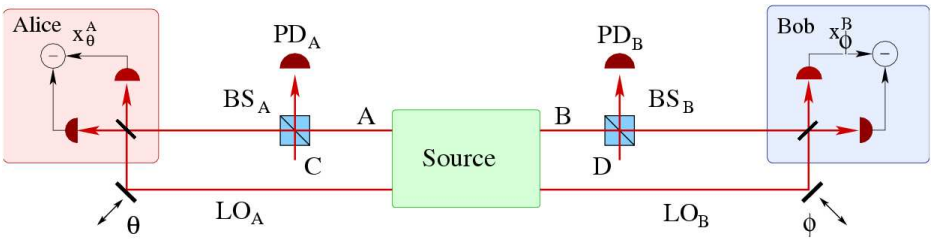

Figure 5.1: *Conceptual scheme for the proposed setup. The source produces two-mode squeezed vacuum in modes A and B, photons are conditionally subtracted at the unbalanced beamsplitters before the homodyne measurement is carried out. The figure is borrowed from [31] and slightly modified from the original version.*

As explained in the motivation, the Gaussian state needs to be de-Gaussified in order to make it possible to break Bell's inequality, this is done by the subtraction of a photon at both beam splitter BS_A and BS_B. The way to insure that one and only one photon is subtracted is to use beam splitters with very high transmittance T. When this is the case, only a tiny part of the light in mode A and B is reflected. The reflected part impinge on a single photon detector, such as an avalanche photodiode.

[3]This can be accomplished by means of non-degenerate parametric amplification in a $\chi^{(2)}$ nonlinear medium or by generating two single-mode squeezed states and mix them on a 50-50 beam-splitter. Details on these can be found in [12, 11].

A successful detection of photons at the photodetectors yields a click. In practice the avalanche photodiodes exhibit a single-photon sensitivity but not a single photon resolution, that is, they can distinguish between the presence and absence of photons but cannot distinguish if there are one, two ore more. This is not a problem as the value of the transmittance T is chosen to be so high that the most possible event leading to a click is that of an single photon being reflected. The probability of two photons entering the detector is smaller by a factor $\approx 1 - T$ which tends to zero in the limit $T \to 1$.

Only the states where two clicks, one in each photodetector, are observed, are used in the Bell statistics. This conditioning on a measurement is a great advantage to us. We choose only to use the states that were prepared successfully and as such we do not have to care about the bad detection efficiency of the avalanche photo detectors. We are however quite vulnerable to dark counts[4], it is therefore important to use a photo detector that is not sensible to these.

5.2.1 Homodyne measurement

In order to examine the resulting state we will perform homodyne measurement of the two modes that are transmitted through the unbalanced beamsplitter. The two modes are sent to Alice and Bob together with a appropriate local oscillator. Alice and Bob then randomly measure $\hat{X}_{A,\theta_j}$, $\hat{X}_{B,\phi_j}$, with $j, k \in \{1, 2\}$. These quadratures are characterized by the relative phases to the local oscillator given by θ_1, θ_2, ϕ_1 and ϕ_2. The rotated quadratures have the following connection to the four quadratures in modes A and B that satisfy $[\hat{X}_n, \hat{P}_m] = i\delta_{n,m}$:

$$\hat{X}_{A,\theta} = \cos(\theta)\hat{X}_A + \sin(\theta)\hat{P}_A \qquad \text{and} \qquad \hat{X}_{B,\phi} = \cos(\phi)\hat{X}_B + \sin(\phi)\hat{P}_B \tag{5.1}$$

These phase displaced quadratures are measured using balanced homodyne detection as explained in the background theory chapter. It is the correlations between these measured quadrature that we will find are in violation with Bell's inequality.

5.3 Realistic model

We will now start to model the setup. We will work in the phase space representation and use Wigner functions. We will find that subtracting photons from the Gaussian two mode squeezed vacuum, transforms the Gaussian Wignerfunction into a Wignerfunction

[4]When a avalanche photo detector click even though no photon is present, it has produced a dark count. Dark count are and their effect on avalanche photo-detectors are described in [32].

that is expressed as a sum of Gaussian functions. This enables us to use all the powerfull tools of quantum optics on the resulting state, even though this is no more expressable as a simple Gaussian state.

In the field of quantum optics, Gaussian states of N modes of light are often encountered. These state are completely specified by their first and second moments of the quadrature operators. The preceding were mentioned in the chapter on Wignerfunctions and are thouroughly explained in [26]. We introduce a vector containing the quadrature operators

$$\hat{R} = (\hat{X}_1, \hat{P}_1, \ldots, \hat{X}_N, \hat{P}_N)^T. \tag{5.2}$$

The different R_k's satisfy $[\hat{X}_j, \hat{P}_k] = i\delta_{j,k}$.

The Wigner function in phase space representation for a N-mode Gaussian state take the form,

$$W(r) = \frac{1}{\pi^N \sqrt{\det \gamma}} \exp[-(r-d)\gamma^{-1}(r-d)] \tag{5.3}$$

In this expression, d is the vector of first moments $\langle \hat{R}_k \rangle$ and γ is the covariance matrix. The vector $r = [X_1, P_1, \ldots, X_N, P_N]^T$ contains the functional dependence on the quadratures of the Wigner function.

The source in the suggested experiment produces two mode squeezed vacuum states, these have all the first moments equal to zero, so the expression can be simplified a bit. We will need to use different covariance matrices: i) for vacuum with displacement vector equal to zero, given by $\gamma_{vac} = I_{2N}$ that is the $2N$ dimensional identity matrix. ii) For a two mode squeezed (TMS) state again with zero displacement, given by

$$\gamma_{TMS} = \begin{bmatrix} \cosh(2s) & 0 & \sinh(2s) & 0 \\ 0 & \cosh(2s) & 0 & -\sinh(2s) \\ \sinh(2s) & 0 & \cosh(2s) & 0 \\ 0 & -\sinh(2s) & 0 & \cosh(2s) \end{bmatrix} \tag{5.4}$$

where s is the squeezing parameter. We will use a different squeezing parameter $\lambda = \tanh s$, the reasons for this are presented in the background theory chapter.

Optical operations that can be implemented with beam splitters, phase shifters and squeezers correspond to Gaussian operations. Their important property is that they map a Gaussian input state onto a Gaussian output state.

Mathematically we can express these kind of transformations, using a mapping $\hat{R} \rightarrow \hat{R}' = S\hat{R}$. Each of the operations thus have a matrix associated with them. For a covari-

ance matrix the transformations have the following effect

$$\gamma \rightarrow S\gamma S^T \tag{5.5}$$

This kind of passive operations will be used throughout this thesis, in particular the following two.

- Mixing two modes of light on a beam splitter with intensity transmittance T and thus reflectance $1-T$. For a two mode state, the transformation matrix can[5] take the form:

$$S_{BS} = \begin{bmatrix} \sqrt{T} & 0 & \sqrt{1-T} & 0 \\ 0 & \sqrt{T} & 0 & \sqrt{1-T} \\ -\sqrt{1-T} & 0 & \sqrt{T} & 0 \\ 0 & -\sqrt{1-T} & 0 & \sqrt{T} \end{bmatrix} \tag{5.6}$$

- A phase shift on a single mode has the following transformation matrix

$$S_{PS}(\theta) = \begin{bmatrix} \cos(\theta) & \sin(\theta) \\ -\sin(\theta) & \cos(\theta) \end{bmatrix} \tag{5.7}$$

5.3.1 Noise

Noisy channels are irreversible quantum operations that cannot be modeled by Gaussian unitary transformations. Instead they can be modeled using tracepreserving Gaussian completely positive maps [8], here the covariance matrix transform as:

$$\gamma \rightarrow A\gamma A^T + G \tag{5.8}$$

Of particular interest of this thesis is the propagation through a lossy channel with transmittance η, which is characterized by $A = \sqrt{\eta}I$ and $G = (1-\eta)I$.

The only place we will include noise in this thesis, is when we model the behavior of imperfect detectors. This is done by having the signal travel through a virtual lossy channels, which is subsequently followed by a perfect detector.

[5] For a proper choice of phases applied, before impingement.

5.4 Wigner function of a two photon subtracted state

Referring to figure 5.1 the two modes A and B are in a two mode squeezed vacuum state while the other two modes, C and D, are in a non-squeezed vacuum state. According to (5.3), we find that the Wigner function for this state is given by

$$W_{in,ABCD} = \frac{1}{\pi^4\sqrt{\det\gamma_{in}}}\exp[-R\gamma_{in}^{-1}R^T] \tag{5.9}$$

with $R = [X_A, P_A, \ldots, X_D, P_D]$ and the covariance matrix γ_{in} is given by

$$\gamma_{in} = \gamma_{TMS,AB} \oplus \gamma_{vac,CD} \tag{5.10}$$

where $\oplus$ denotes the direct sum of the matrices. The imperfect single photo detectors are modeled using η_{PD}, which will serve as a measure of the efficiency of the photo detectors. In our setup the modes A and C (B and D) are mixed using an unbalanced beam splitter and passed through four virtual lossy channels before impinging on the photo-detectors. The covariance matrix transform as

$$\gamma_{out} = S_\eta S_{mix}\gamma_{in}S_{mix}^T S_\eta^T + G \tag{5.11}$$

where

$$S_\eta = \sqrt{\eta_{BHD}}I_{AB} \oplus \sqrt{\eta_{PD}}I_{CD} \tag{5.12}$$

$$G = (1-\eta_{BHD})I_{AB} \oplus (1-\eta_{PD})I_{CD} \tag{5.13}$$

$$S_{mix} = S_{BS,AC} \oplus S_{BS,CD} \tag{5.14}$$

S_{mix} describes the mixing of the A and C (B and D) mode on the unbalanced beam splitters BS_A (BS_B), respectively. γ_{out} is the covariance matrix of the system just before we detect two clicks in the photo detectors. The Wigner function becomes

$$W_{out,ABCD} = \frac{1}{\pi^4\sqrt{\det\gamma_{out}}}\exp[-R\gamma_{out}^{-1}R^T]. \tag{5.15}$$

5.4.1 Two photon subtraction

The photo-detectors only measure if there are photons or not, they do not count photons. The effect of such a detector can be modeled as the effect of a projection of the state onto either vacuum $\hat{\Pi}_0 = |0\rangle\langle 0|$ or on the rest of the Hilbert space $\hat{\Pi}_1 = I - |0\rangle\langle 0|$. $\hat{\Pi}_0$ and $\hat{\Pi}_1$ referring to no click and click respectively. We wish to subtract photons from the modes

and are therefore interested in obtaining clicks in the detectors, we will thus use $\hat{\Pi}_1$. The resulting density matrix for A,B takes the form

$$\hat{\rho}_{c,AB} = \mathrm{Tr}_{CD}[\hat{\rho}_{out,ABCD}(\hat{I}_{AB} \otimes \hat{\Pi}_{1,C} \otimes \hat{\Pi}_{1,D})] \tag{5.16}$$

the subscript c on $\hat{\rho}_{c,AB}$ refers to conditionally prepared. The operator acting on $\hat{\rho}_{out,ABCD}$ leave mode A and B unchanged and subtracts one photon from modes C and D. In the chapter on Wignerfunctions we found that a trace of this form, can be rewritten as an integral over the Wignerfunctions of the operators. Using this we get that

$$\hat{\rho}_{c,AB} = (2\pi)^2 \int dCdD\, W_{out,ABCD}(\hat{r}) W_{\hat{I}_{AB}\otimes\hat{\Pi}_{1,C}\otimes hat\Pi_{1,D}}(\hat{r}) \tag{5.17}$$

Here $dC = d\hat{X}_C d\hat{P}_C$ and likewise for dD. The functional argument $\hat{r}$ is now partly a number for modes C, D and partly operator in modes A,B

$$\hat{r} = [\hat{X}_A, \hat{P}_A, \hat{X}_B, \hat{P}_B, X_C, P_C, X_D, P_D]^T. \tag{5.18}$$

The Wigner function for the three operators $\hat{I}_{AB} \otimes \hat{\Pi}_{1,C} \otimes \hat{\Pi}_{1,D}$ is simply the product of the three Wigner functions representing of each of the operators. The individual Wigner functions are calculated in appendix B, for single modes they are found to be

$$W_{|0\rangle\langle 0|} = \frac{1}{\pi}\exp[-\hat{r}^T I \hat{r}] \qquad \text{and} \qquad W_I = \frac{1}{2\pi} \tag{5.19}$$

The product of the three[6] Wigner functions is then found to be

$$\begin{aligned} W_{\hat{I}_{AB}\otimes\hat{\Pi}_{1,C}\otimes\hat{\Pi}_{1,D}}(\hat{r}) &= W_{\hat{I}}(\hat{A}) W_{\hat{I}}(\hat{B}) W_{\hat{\Pi}_1}(C) W_{\hat{\Pi}_1}(D) \\ &= \frac{1}{(2\pi)^2}\left(\frac{1}{2\pi} - \frac{1}{\pi}e^{-C^T I C}\right)\left(\frac{1}{2\pi} - \frac{1}{\pi}e^{-D^T I D}\right) \\ &= \frac{1}{(2\pi)^4}\left(1 - 2e^{-C^T I C} - 2e^{-D^T I D} + 4e^{-C^T I C - D^T I D}\right) \end{aligned} \tag{5.20}$$

Where, for example, C refers to the vector $[X_C, P_C]^T$ and so forth. Finding the integrand of equation (5.17) amounts to multiplying equations (5.20) and (5.15).

We will now introduce some new notation that will be usefull in the following calculations. The coefficients in the sum in (5.20) will be denoted q_j with $q_1 = 1$, $q_2 = q_3 = -2$ and $q_4 = 4$. Setting $\gamma_{out}^{-1} = \Gamma$ we can divide the symmetric[7] $[8 \times 8]$-matrix up in four

[6] The Wigner function for I_{AB} is simply the product of two single mode Wignerfunctions for the identity.
[7] This property is a result of the definition of the covariance matrix.

matrices, each of dimension $[4 \times 4]$

$$\Gamma = \begin{bmatrix} \Gamma_{AB} & \sigma \\ \sigma^T & \Gamma_{CD} \end{bmatrix} \tag{5.21}$$

The product of the two Wignerfunctions in equation (5.17) can now be expressed as

$$\frac{1}{2^4\pi^8\sqrt{\det\gamma_{out}}}\sum_{j=1}^{4} q_j \exp\left[-\hat{r}^T \begin{bmatrix} \Gamma_{AB} & \sigma \\ \sigma^T & \Gamma_{j,CD} \end{bmatrix} \hat{r}\right] \tag{5.22}$$

with the $\Gamma_{j,CD}$ given by

$$\begin{aligned} \Gamma_{1,CD} &= \Gamma_{CD} & \Gamma_{2,CD} &= \Gamma_{CD} + I_C \otimes 0_D \\ \Gamma_{3,CD} &= \Gamma_{CD} + 0_C \otimes I_D & \Gamma_{4,CD} &= \Gamma_{CD} + I_{CD} \end{aligned} \tag{5.23}$$

Comparing to the integral we are trying to solve, (5.17), we now see that we have a sum of Gaussian forms, instead of just one. We know how to do the integral for each of the terms in the sum, the procedure is explained in appendix A.

Doing the integral we find that the density matrix for the two photon subtracted state has the form

$$\hat{\rho}_{c,AB} = \frac{1}{4\pi^4\sqrt{\det\gamma_{out}}}\sum_{j=1}^{4}\frac{q_j}{\sqrt{\det\Gamma_{j,CD}}}\exp[-\hat{r}'^T(\Gamma_{AB} - \sigma\Gamma_{j,CD}^{-1}\sigma^T)\hat{r}'] \tag{5.24}$$

where $\hat{r}' = [\hat{X}_A, \hat{P}_A, \hat{X}_B, \hat{P}_B]^T$. In order of simplifying the expression a bit we introduce $\Gamma_{j,AB} = \Gamma_{AB} - \sigma\Gamma_{j,CD}^{-1}\sigma^T$.

5.4.2 Finding the Wigner function

The Wigner function for the photonsubtracted state is now easily found. We apply the definition of a Wigner function to the density operator found above in equation 5.24

$$\begin{aligned} \tilde{W}_{c,AB} = \frac{1}{(2\pi)^2}\int dx'dx''\langle X_A - \frac{x'}{2}, X_B - \frac{x''}{2}|\hat{\rho}_{c,AB}|X_A + \frac{x'}{2}, \\ X_B + \frac{x''}{2}\rangle \exp[i(P_Ax' + P_Bx'')] \end{aligned} \tag{5.25}$$

When finding the Wigner function of a Gaussian density operator, as the one we found in 5.24, we simple calculate it as if the operators where scalars. This is a well known property used throughout the literature, a proof of this can be found in [25].

This simplifies the evaluation of the integral 5.25 a great deal

$$\tilde{W}_{c,AB} = \frac{1}{(2\pi)^2} \int dx' dx'' \rho_{c,AB} \delta(x') \delta(x'') \exp[i(P_A x' + P_B x'')] \tag{5.26}$$

yielding $\tilde{W}_{c,AB} = (2\pi)^{-2} \rho_{c,AB}$, where $\rho_{c,AB}$ now is to be understood as a function of $X_A, \ldots, P_B$.

5.4.3 Normalization

Having subtracted photons from the two modes, we find that the resulting Wigner function are now unnormalized. The tilde-symbol ($\sim$) on top of $\tilde{W}_{c,AB}$ refers to the fact that the Wigner function here is still unnormalized. To do the normalization we integrate the Wigner function over the entire phase space, and demand that the result is 1. We will introduce a constant P_G that insures this.

We do the integral $\int dX_A dP_A dX_B dP_B \; W_{c,AB}$ using appendix A and find that we can define

$$P_G = \det[\gamma_{out}]^{-1/2} \sum_{j=1}^{4} q_j (\det[\Gamma_{j,AB}] \det[\Gamma_{j,CD}])^{-1/2}, \tag{5.27}$$

which is the probability of a successful conditional preparation of the state. The resulting normalized Wigner function is.

$$W_{c,AB} = \frac{1}{\pi^2 P_G \sqrt{\det \gamma_{out}}} \sum_{j=1}^{4} \frac{q_j}{\sqrt{\det \Gamma_{j,CD}}} \exp[-r'^T \Gamma_{j,AB} r'] \tag{5.28}$$

From the normalized Wignerfunction of the two photon subtracted state (shown above) we can calculate all the information we need about the state. It is this state that will be shown to be cabable of breaking Bell's inequality. We will start by finding the joint probability function. The Joint probability function associates probabilities to the different measuring outcomes of measurements of $\hat{X}_A$ and $\hat{X}_B$ and can be used to find the correlation coefficient in Bell's inequality.

5.5 Joint probability distribution

In the section on Bell's inequality we found that for a given experiment there are probabilities associated with different outcomes of measurements. In order to test Bell's inequality we need to find these probabilities for two sets of randomly imposed parameters, our parameters are the phases.

We do homodyne measurement of the quadratures ($\hat{X}_A$ and $\hat{X}_B$) on both Alice's and Bobs part of the state. The measurements are performed at a set of randomly imposed set of phases ($\theta_{1,2}$ and $\phi_{1,2}$).

The effect of the phases is that we actually measure a set of rotated phases, which relate in the following way to the original phases

$$\hat{X}_{A,\theta_j} = \cos(\theta_j)\hat{X}_A + \sin(\theta_j)\hat{P}_A \tag{5.29}$$

$$\hat{X}_{B,\phi_k} = \cos(\phi_k)\hat{X}_B + \sin(\phi_k)\hat{P}_B. \tag{5.30}$$

The application of the phases are modelled by multiplying a phase shift matrix on to the vector containing the quadratures; $r_{\theta_j,\phi_k} = [X_{A,\theta_j}, P_{A,\theta_j}, X_{B,\phi_k}, P_{B,\phi_k}]^T$.

$$S_{sh,jk} = \begin{bmatrix} \cos\theta_j & \sin\theta_j & 0 & 0 \\ -\sin\theta_j & \cos\theta_j & 0 & 0 \\ 0 & 0 & \cos\phi_k & \sin\phi_k \\ 0 & 0 & -\sin\phi_k & \cos\phi_k \end{bmatrix} \tag{5.31}$$

We saw in the chapter on Wigner functions that the probability of finding the system in a state with quadrature component q is given by $|\psi(q)|^2 = \int dp W(p,q)$. The joint probability function can be found in the same way - also invoking the phase shift we find

$$P(X_{A,\theta_j}, X_{B,\phi_k}) = \int dP_{A,\theta_j} dP_{B,\phi_k}\, W_{c,AB}(S^T_{sh,jk} r) \tag{5.32}$$

To do this integral we once again turn to appendix A. The result of appendix A can be directly applied if we rearrange the order of the quadrature phases. This is easily done using a matrix, that we will call S_{hom} given by

$$\begin{bmatrix} X_{A,\theta_j} \\ X_{B,\phi_k} \\ P_{A,\theta_j} \\ P_{B,\phi_k} \end{bmatrix} = \begin{bmatrix} 1 & 0 & 0 & 0 \\ 0 & 0 & 1 & 0 \\ 0 & 1 & 0 & 0 \\ 0 & 0 & 0 & 1 \end{bmatrix} \begin{bmatrix} X_{A,\theta_j} \\ P_{A,\theta_j} \\ X_{B,\phi_k} \\ P_{B,\phi_k} \end{bmatrix} \tag{5.33}$$

The subscript *hom* refers to homogeneous, in the sense that it is really the same matrix, the order of the rows are just switched.

Then we are ready to use appendix A on the matrix with phases and homogeneous

reordering applied to it

$$\Gamma'_{j,AB} = S_{hom} S_{sh,jk} \Gamma_{j,AB} S^T_{sh,jk} S^T_{hom} = \begin{bmatrix} A_j & C_j \\ C_j^T & B_j \end{bmatrix} \tag{5.34}$$

we have split the matrix in submatrices all are of dimensions $[2 \times 2]$, these will be used momentarily. We find the joint probability function to be

$$P(X_{A,\theta_j}, X_{B,\phi_k}) = \frac{1}{\pi P_G \sqrt{\det \gamma_{out}}} \sum_{j=1}^{4} \frac{q_j}{\sqrt{\det \Gamma_{j,CD} \det B_j}} \exp[-y^T \Gamma_j y] \tag{5.35}$$

where we have defined the vector $y = [X_{A,\theta_j}, X_{B,\phi_k}]^T$ and $\Gamma_j = A_j - C_j B_j^{-1} C_j^T$.

We can plot this for a given set of parameters $\lambda, T, \eta_{PD}, \eta_{BHD}, \theta_j$ and ϕ_k as a function of $\hat{X}_{A,\theta_j}$ and $\hat{X}_{B,\phi_k}$, see figure 5.5.

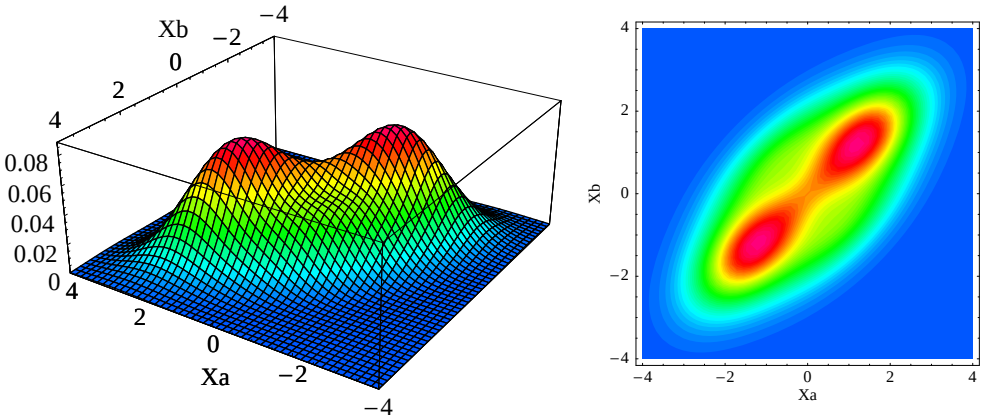

Figure 5.2: *Joint probability distribution for a state with $\lambda = 0.6$, $\eta = 1$, $T = 0.99$ and for the phases $\theta = 0$, $\phi = \pi/4$. It is easy to see that Alice and Bob should expect strongly correlated measurements.*

We can see from the joint probability distribution that the two peaks are placed such that it is very likely that Alice and Bob either measure both quadratures positive or both quadratures negative. We see this behavior for three of the four sets of phase angles, for the fourth the coorelations is opposite. Opposite meaning, that it is very likely that Alice and Bob find opposite signs on their quadratures when they both perform measurements on their part of the state.

The next step is to get a quantitive description of the correlation, and not just the qualitative that the plot offers. As discussed earlier we need to measure the level of entanglement between the states of Alice and Bob, we will do this by calculating the Bell

coefficient S_{Bell}. In order to do this calculation for a continuous variable system we need to discretize the outcomes through the process of sign-binning.

5.6 Sign-binning

In the the discrete case we can calculate the correlation coefficient $E(\theta_j, \phi_k)$ given by doing a weighted sum of probabilities

$$E(\theta_j, \phi_k) = +P(1,1|\theta_j, \phi_k) + P(-1,-1|\theta_j, \phi_k) - P(1,-1|\theta_j, \phi_k) - P(-1,1|\theta_j, \phi_k). \tag{5.36}$$

In the case of continuous variables the outcome of measurements form a continuum, we therefore need another way of calculating $E(\theta_j, \phi_k)$. If we associate a measurement of $\hat{X} \geq 0$ with $+1$ and a measurement of $\hat{X} < 0$ with -1, then we can see that the following equation must be the continuous variables counterpart of 5.36.

$$E(\theta_j, \phi_k) = \int d\hat{X}_{A,\theta_j} d\hat{X}_{B,\phi_k} \text{sign}(\hat{X}_{A,\theta_j} \hat{X}_{B,\phi_k}) P(\hat{X}_{A,\theta_j}, \hat{X}_{B,\phi_k}) \tag{5.37}$$

It is easy to see that the joint probability distribution is symmetric $P(\hat{X}_{A,\theta_j}, \hat{X}_{B,\phi_k}) = P(-\hat{X}_{A,\theta_j}, -\hat{X}_{B,\phi_k})$. Earlier we made sure that the joint probability distribution was also normalized $\int d\hat{X}_{A,\theta_j} d\hat{X}_{B,\phi_k} P(\hat{X}_{A,\theta_j}, \hat{X}_{B,\phi_k}) = 1$. These two realizations can be used to simplify the integral a bit. Manipulating with the limits of integration [8] and using the two aforementioned properties we can restate the integral as

$$E(\theta_j, \phi_k) = 4 \left[\int_0^\infty \int_0^\infty d\hat{X}_{A,\theta_j} d\hat{X}_{B,\phi_k} P(\hat{X}_{A,\theta_j}, \hat{X}_{B,\phi_k}) \right] - 1. \tag{5.38}$$

This is an reasonably easy calculation. Each of the 4 matrices Γ_j's, from the joint probability distribution, can be split up using the following notation

$$\Gamma_j = \begin{bmatrix} a_j & c_j \\ c_j & b_j \end{bmatrix}. \tag{5.39}$$

[8] Using a simplified notation we get where all the integrations are with respect to $d\hat{X}_{A,\theta_j} d\hat{X}_{B,\phi_k}$, and P denotes the joint probability distribution, the integral can be evaluated as

$$\int_{-\infty}^{\infty}\int_{-\infty}^{\infty} \text{sign}(\hat{X}_A \hat{X}_B) P = \left(\int_0^\infty \int_0^\infty + \int_{-\infty}^0 \int_{-\infty}^0 - \int_0^\infty \int_{-\infty}^0 - \int_{-\infty}^0 \int_0^\infty \right) P$$
$$= \left(2\int_0^\infty \int_0^\infty - 2\int_0^\infty \int_{-\infty}^0 + \int_{-\infty}^\infty \int_{-\infty}^\infty \right) P - 1 = 4 \left[\int_0^\infty \int_0^\infty d\hat{X}_A d\hat{X}_B P \right] - 1$$

It will be helpfull to introduce a new parameter G_j that consists of the integral

$$G_j = \int_0^\infty \int_0^\infty dy_1 dy_2 \exp[-a_j y_1^2 - b_j y_2^2 - 2c_j y_1 y_2]. \tag{5.40}$$

This integral can most easily be done by switching to polar coordinates. Starting with the radial integral followed by the angle integral, we can find that

$$G_j = \frac{1}{2\sqrt{\det \Gamma_j}} \left[\frac{\pi}{2} - \arctan \frac{c_j}{\sqrt{\det \Gamma_j}} \right] \tag{5.41}$$

Now it is straight forward to calculate $E(\theta_j, \phi_k)$

$$E(\theta_j, \phi_k) = \frac{4}{\pi P_G \sqrt{\det \gamma_{out}}} \left[\sum_{j=1}^{4} \frac{q_j G_j}{\sqrt{\det \Gamma_{j,CD} \det B_j}} \right] - 1 \tag{5.42}$$

and from this we can get the Bell parameter as follows

$$S_{Bell} = |E(\theta_1, \phi_1) + E(\theta_1, \phi_2) + E(\theta_2, \phi_1) - E(\theta_2, \phi_2)| \tag{5.43}$$

If $S_{Bell} \geq 2$ then the correlations in the system are stronger than any classical theory would permit. We now have all the tools needed to calculate the properties we seek in the conditionally prepared state. The following section will present the results.

5.7 The conditionally prepared state

Just as in the article by R. García-Patrón, J. Fiurásek and N.J. Cerf [8] we find that the choice of angles that give the highest degree of correlation is given by $\theta_1 = 0$, $\theta_2 = \pi/2$, $\phi_1 = -\pi/4$ and $\phi_2 = \pi/4$, the results in this section are shown for these values. Firstly we can plot a cross-section of the Wignerfunction, showing that we have some part of it that is negative. If the Wignerfunction were completely nonnegative we could not have had any violation of Bells inequality. We see that the negative area is small so we should not expect a high violation of Bells inequality for this state.

To examine the parameterspace we let the squeezing parameter λ vary over a range for three different values of T. T is the transmittance of the beamsplitter that subtracts photons, we use the values $T = 0.9$, $T = 0.95$ and $T = 0.99$. We see that we have a maximal violation for an optimal choice of λ given by $\lambda_{obt} T \approx 0.57$.

For $T = 0.99$ we can get $S_{bell} = 2.045$. This is equivalent to a violation of Bell's inequality of about 2.2%, which is definitely a strong enough violation that it conclusively

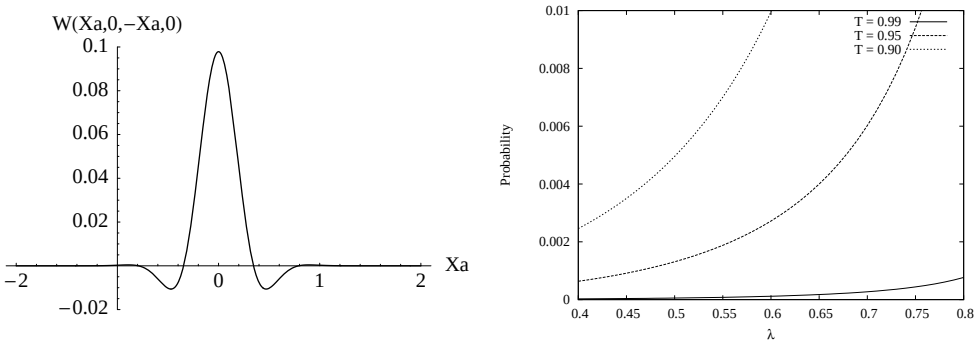

Figure 5.3: *On the left side there is a plot of the Wigner function for $\hat{P}_A = \hat{P}_B = 0$, and $\hat{X}_B = -\hat{X}_A$, the transmittance is $T = 0.99$ and $\lambda = 0.6$. We see that the negative area is small so we do not expect a large violation of Bell's inequality. On the right side there is the probability for successful generation of the photon subtracted state. We see that the probability is strongly dependent on T.*

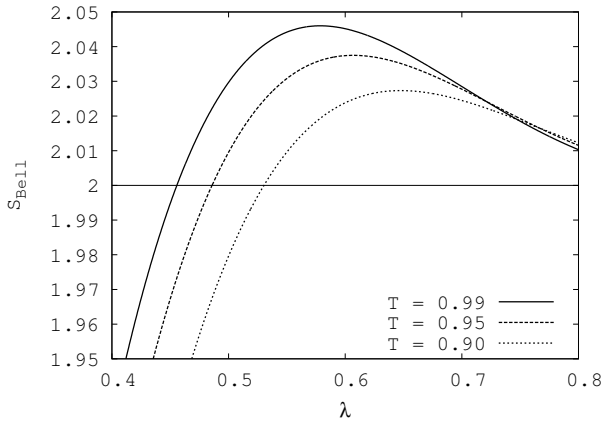

Figure 5.4: *Plot of the violation of Bell's inequality for different different levels of transmittance and varying λ. We find that the peaks are situated at approximately $\lambda T = 0.57$. The violation of Bell is in the percent range.*

can be proven that Bell is violated. In [8] they state that *"with a repetition rate of 1 MHz and $P \approx 2.6x10^{-4}$, the number of data samples would be several hundreds per second, so that the required statistics to see a violation in the percent range could be obtained in a reasonable time (a few hours)"*.

It is clear from the graph that we get a better violation of Bell's inequality for higher values of T. But if we plot the probability of a successful preparation, denoted P_G, we see that it scales with T, see figure 5.3. There is a tradeoff between getting a high violation and getting a conditionally prepared state and thereby a successful experiment. In an experimental setup such a tradeoff should be carefully considered before making measurements.

In figure 5.4 the Bell parameter is plotted for a set of high values of the transmitivity, of the beamsplitter that leads part of the beam onto a photo detector. If we choose a too low value for T then it is impossible to break Bell's inequality. The reason for this is, the output from the beamsplitters gets contaminated with the vacuum modes. We see that depending on the amount of squeezing, λ, the Bell parameter peaks, this is also expected. The mean photon number increases with the squeezing λ, and at large squeezing numbers the projection on $I - |0\rangle\langle 0|$ brings little change to the state.

5.7.1 Experimental imperfections

We will now look at the influence the different experimental imperfections in the system, have on the Bell parameter. We can plot the Bell parameter as a function of the detectionefficiency of the photo detectors η_{PD}. We plot for the optimal choice of squeezing, T=0.99 and keeping the efficiency of the balanced homodyne detection$\eta_{BHD} = 1$, see figure 5.5.

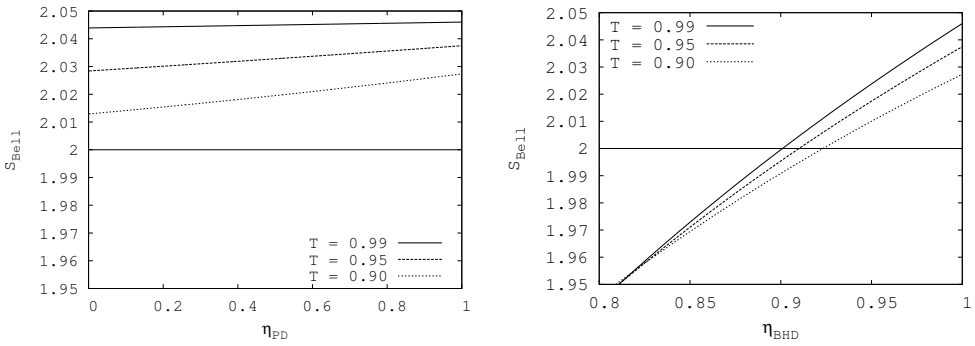

Figure 5.5: *Plot of the dependency on of the efficiency of the photo-detection and the balanced homodyne detection respectively. Both plots are made for three different values of transmittance, T.*

We see that the dependence on the photo-detectors efficiency is very weak. This is a good thing as the avalanche photo detectors there is available today work at an efficiency of about 50%. We can conclude that using realistic photodetection efficiency values we would still expect a violation of Bell's inequality of the same order as with perfect detectors. This is not a big surprise, as the effect of the photo detectors only is to conditionally generate the non-Gaussian state. The result of a low detector efficiency would be a longer time spend waiting in the laboratory, before the wanted number of conditionally prepared states have been collected..

Doing the same plot for the balanced homodyne detection efficiency, with the same choices of squeezing and T, we arrive at figure 5.5. The optimal squeezing parameter is dependent on the efficiency η_{BHD}, but this plot is done for a fixed value. It is therefore possible to obtain better results[9] than what is shown above, but it will lead to the same conclusion

The dependency on the balanced homodyne detectors is much more critical than what we found for the photodetectors. We see that we need to have an efficiency in the order of 90%, to have an violation of the Bell inequality. Efficiencies of about $90 - 95\%$ have already been achieved experimentally.

5.8 Summary

Following the work presented in [8, 30, 31], we found that it was possible to construct a state that breaks Bell's inequality in a loophole free setting. We did this using beamsplitters and photodetectors. The specifications, η_{BHD}, η_{PD} and λ, needed for a violation of Bell's inequality, all are within reach of modern day experiments. In the article by Garcia-Patron et al. [8] they found that it is possible to see a violation of Bell's inequality in the percent range after an hour of observation.

The Bell violation is very weakly dependent on the photo-detection efficiency as this only serve to prepare the state. But we need a high-efficiency balanced homodyne detector $\eta_{BHD} \approx 90 - 95\%$, in order to see Bell violation.

The probability for a successful two photon subtraction is found to be very strongly dependent on T, this is an important factor to consider in an experiment.

The calculations that we have done in this chapter are typical to the remainder of this thesis, using Wigner functions for Gaussian operators we were able to reduce all the calculations to linear algebra. All the numerical work was done using Mathematica,

[9] We have found that it is possible to compensate a bit for the imperfections in the balanced homedyne detection by increasing the amount of squeezing.

see appendix D for a list of the Mathematica programs used. In these programs it was possible to search the parameter spaces for an optimal choice of phases.

Chapter 6

Purification procedure

In this chapter we will use the results of the previous chapter to propose a purification method for the resulting two mode photon subtracted state. We will at this point start to use the abbreviation TMPS (Two Mode Photon Subtracted). In particular we will use the properties of the JP (Joint Probability) distribution for the TMPS state to draw an analogy to the $|\phi^+\rangle$-Bell state in the qubit basis. The Bell states will be introduced as well.

Deutsch et Al. [9] have suggested a purification protocol for Bell states, which is particularly easy to implement for the $|\phi^+\rangle$ state. We will present details explaining how this protocol works.

We will argue, that a continuous variable version of the qubit purification protocol by Deutsch can be made, which should work for the TMPS state. In this chapter we will not concern ourselves with detailed calculations, but rather focus on what parts and concepts that needs to be incorporated in order to model and construct the suggested purification protocol.

6.1 Interpretation of the JP distribution for the TMPS state

We are free to impose phases on the TMPS state, we saw in the previous chapter that it is possible to choose these angels such that JP distribution take the shapes as shown below in figure 6.1. The plots are shown for the set of angles that led to the maximum violation of Bell's inequality.

We are interested in choosing phases such that Alice and Bob with a high probability would agree on the sign on their measured quadratures. This is indeed possible as this is the case for the first three plots. On the fourth of the plots in figure 6.1, we have chosen phases such that the Alice and Bob would find opposite quadrature sign correlations.

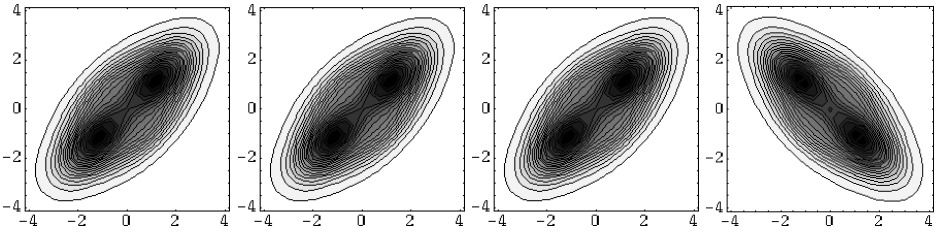

Figure 6.1: *Plot of the four joint probability distributions for the choice of phases that led to a maximum violation of Bell's inequality. The two axis are X_A and X_B respectively. The four set of phases are $(\theta, \phi) = \{(0, -\pi/4), (0, \pi/4), (\pi/2, -\pi/4), (\pi/2, \pi/4)\}$.*

The TMPS state with phases such that Alice and Bob will agree on the sign on a measurement of quadratures could be represented as

$$|\psi\rangle \approx \frac{1}{\sqrt{2}}(|X_{A,+}X_{B,+}\rangle + |X_{A,-}X_{B,-}\rangle). \tag{6.1}$$

Here we have adopted the nomenclature that $|X_{A,+}\rangle$ denotes that Alice measure her $\hat{X}$-quadrature positive. The reason for the $\approx$ is due to the small part of the JP distribution that exists in the two quadrants where $\hat{X}_A$ and $\hat{X}_B$ have a different sign. We can see from figure 6.1, that this part is small so we almost have an equalitysign in 6.1.

The meaning of 6.1 inspire us to draw the analogy to one of the qubit Bell states[1], namely $|\phi^+\rangle = 2^{-1/2}(|00\rangle_{AB} + |11\rangle_{AB})$. Analogous to the TMPS state this state also finds Alice and Bob agreeing on their measurements, either both measuring 1 or both measuring 0.

We would like to know if there were more features shared by the $|\phi^+\rangle$ Bell state and the TMPS state. Hoping to find such features we could try to represent the qubit state $|\phi^+\rangle$ in the spin-1/2 basis with 1 and 0 representing up and down in the z-basis respectively. In this case we see that measuring the $\hat{X}$-quadrature in the two photon subtracted state is analogous to measuring the z component of the spin in the $|\phi^+\rangle$-Bellstate. If we were to measure the the $\hat{P}$-quadrature instead[2], we would obtain the opposite correlation, that is we get $\hat{P}_A = -\hat{P}_B$. This is completely analogous to making a measurement of the y-component of the spin in the $|\phi^+\rangle$-qubit state. If we represent $|\phi^+\rangle$ in the y basis we get $|\uparrow\uparrow\rangle_{AB,z} + |\downarrow\downarrow\rangle_{AB,z} = |\uparrow\downarrow\rangle_{AB,y} + |\downarrow\uparrow\rangle_{AB,y}$

We see that there is a range of similarities between the Bell state $|\phi^+\rangle$ and the TMPS state. We wish to utilize this when constructing the purification protocol, for the two photon subtracted state.

[1]The entire set of Bell states will be introduced below.

[2]We can apply a phase of $\pi/2$ to both the A and B mode and obtain the JP distribution for PA and PB.

Deutsch et al. [9] have proposed a purification method, that is able to purify any Bell state. The proposed protocol is the simplest for the aforementioned $|\phi^+\rangle$-state, it uses a few simple operations and will prove very effective. We hope that knowledge of this protocol can help us to construct a continuous variable analogy to purify the TMPS states.

6.2 Qubit purification protocol by Deutsch et al.

Alice and Bob have a supply of qubit-pairs. Each pair is prepared such that the probability of finding it in the maximally entangled $|\phi^+\rangle$ Bell state is large. The Bell states form a convenient basis for the space of qubit-pairs, the complete set of Bell states consits of:

$$\begin{aligned} |\phi^+\rangle &= \frac{|00\rangle_{AB} + |11\rangle_{AB}}{\sqrt{2}} & |\phi^-\rangle &= \frac{|00\rangle_{AB} - |11\rangle_{AB}}{\sqrt{2}} \\ |\psi^+\rangle &= \frac{|01\rangle_{AB} + |10\rangle_{AB}}{\sqrt{2}} & |\psi^-\rangle &= \frac{|01\rangle_{AB} - |10\rangle_{AB}}{\sqrt{2}} \end{aligned} \tag{6.2}$$

It is hard to produce a perfect $|\phi^+\rangle$-state experimentally, added to this difficulty is the presence of noise and the fact that qubit states cannot be perfectly isolated from the surroundings. The result is that entanglement is produced between the states and the environment. The sum of all these effects drives the $|\phi^+\rangle$ state into a superposition of all the Bell states (6.2). The idea behind the purification protocol, is to drive the state back towards the pure state described by the $|\phi^+\rangle$ state.

In order to do this we need two qubit pairs. We send one qubit from each pair to Alice and one from each pair to Bob.

The first step in the protocol is that Alice performs the unitary operation,

$$|0\rangle_A \rightarrow \frac{1}{\sqrt{2}}(|0\rangle_A - i|1\rangle_A) \qquad |1\rangle_A \rightarrow \frac{1}{\sqrt{2}}(|1\rangle_A - i|0\rangle_A) \tag{6.3}$$

on each of her qubits and Bob performs the inverse operation on his qubits.

$$|0\rangle_B \rightarrow \frac{1}{\sqrt{2}}(|0\rangle_B + i|1\rangle_B) \qquad |1\rangle_B \rightarrow \frac{1}{\sqrt{2}}(|1\rangle_B + i|0\rangle_B). \tag{6.4}$$

If the qubits are spin-$\frac{1}{2}$ particles and the qubit basis is that of the eigenstates of the z-components of their spin, then these operations correspond to rotations about the x-axis of $\pi/2$ and $-\pi/2$ respectively. This operation does the following to the four Bell states,

$$\begin{aligned} |\phi^+\rangle &\rightarrow |\phi^+\rangle & |\phi^-\rangle &\rightarrow i|\psi^-\rangle \\ |\psi^+\rangle &\rightarrow |\psi^+\rangle & |\psi^-\rangle &\rightarrow i|\phi^-\rangle. \end{aligned} \tag{6.5}$$

We find that $|\phi^+\rangle$ and $|\psi^+\rangle$ are unchanged while the other two to are interchanged and a phase is added.

The first part of the purification protocol is no more than a rotation in phase space. Which is equivalent to a change of phase on the qubits.

6.2.1 Controlled-NOT operation

The second part of the purification protocol, consists of a controlled-NOT operation. This is where the actual purification takes place, the controlled-NOT looks for deviations from the $|\phi^+\rangle$-state, and discards the states that differ from this.

The controlled-NOT (cNOT) does the following to a qubit pair,

$$\underbrace{|x\rangle}_{\text{control}}\ \underbrace{|y\rangle}_{\text{target}} \rightarrow \underbrace{|x\rangle}_{\text{control}}\ \underbrace{|x \oplus y\rangle}_{\text{target}} \qquad (x, y) \in \{0, 1\}. \tag{6.6}$$

Alice and Bob perform two quantum controlled-NOT gate operations, where the first qubit is the control and the second is the target. The two control qubits and the two target qubits should pair for pair form the original qubit pairs sent from the source.

After the cNOT, Alice and Bob both measure the target qubits in the computational basis (for example: the z-component of their targets spin). If Alice and Bob find that the targets coincide, then they keep the control pair and discard the target pair. If the targets do not coincide, then both pairs are discarded.

The effect of this protocol to a set of qubit pairs can be explained by calculating the effect on the $|\phi^+\rangle$ state. Let $|\phi_c\rangle = |00\rangle_{AB} + |11\rangle_{AB}$ denote the control pair and $|\phi_t\rangle = |00\rangle_{AB} + |11\rangle_{AB}$ denote the target pair, both pairs are prepared in the $|\phi^+\rangle$ Bell state. In this section we have omitted all the normalizing factors of $\sqrt{2}$, as these do not influence the result. The joint state is formed as the product of the two states presented above,

$$|\psi\rangle = |\phi_c\rangle|\phi_t\rangle = |00\rangle_A|00\rangle_B + |01\rangle_A|01\rangle_B + |10\rangle_A|10\rangle_B + |11\rangle_A|11\rangle_B \tag{6.7}$$

both Alice and Bob now let the cNOT act on their qubit pairs, $|\tilde{\psi}\rangle = cNOT_A cNOT_B|\psi\rangle$, the result of this is

$$|\tilde{\psi}\rangle = |00\rangle_A|00\rangle_B + |01\rangle_A|01\rangle_B + |11\rangle_A|11\rangle_B + |10\rangle_A|10\rangle_B, \tag{6.8}$$

the state is thus left unchanged by the cNOTs.

In this perfect case, we can see that if Alice and Bob both measure their target qubits,

then their results will always coincide. We find that the resulting state shared by Alice and Bob after they have discarded the target pairs, independent of whether Alice and Bob both measure 0 or 1, will collapse to the $|\phi^+\rangle$. We have thus seen that both steps of the protocol leaves the $|\phi^+\rangle$-Bellstate "unharmed", this is an essential feature as this is the state we wish to preserve and thus purify.

The action of the controlled-NOT is effectively a method for error finding. When we have ensemble of states, then it is the the elimination of the states with an error occuring that leads to the purification on average in the ensemble.

To see this effect we let the cNOTs act on a pair of qubit states where a bit flip has occurred just before the cNOTs are applied, $|0\rangle \leftrightarrow |1\rangle$. If we let the bit flip occur in the control qubit pair[3], $\tilde{\phi_c} = |01\rangle_{AB} + |10\rangle_{AB}$, we see that we have the following joint state.

$$|\Psi\rangle = \tilde{\phi_c}\phi_t = |00\rangle_A|10\rangle_B + |01\rangle_A|11\rangle_B + |10\rangle_A|00\rangle_B + |11\rangle_A|01\rangle_B \tag{6.9}$$

Having the cNOTs applied to this state, we obtain

$$|\tilde{\Psi}\rangle = |00\rangle_A|11\rangle_B + |01\rangle_A|10\rangle_B + |11\rangle_A|00\rangle_B + |10\rangle_A|01\rangle_B \tag{6.10}$$

we see now that if Alice and Bob each were to measure their target qubit they would newer agree on the result and therefore discard the resulting control pair. When a bitflip has occurred, Alice and Bob are able to see the error and remove the error infected state, exactly as wanted.

Instead of a large bit flip we could imagine a bit flip occurring with a small probability proportional to ϵ such that $|0\rangle \rightarrow |0\rangle + \epsilon|1\rangle$ and $|1\rangle \rightarrow |1\rangle - \epsilon|0\rangle$. In this case the resulting state after the cNOTs is in a superposition similar to $|\tilde{\psi}\rangle + \epsilon|\tilde{\Psi}\rangle$. In some fraction of the outcomes, proportional to ϵ, we would have Alice and Bob getting different results in the measurement of their target qubits, thus discarding the control pairs. In the rest of the outcomes they would keep the control pair which now would be in the $|\phi^+\rangle$-state.

6.2.2 Quantitative results

To see the effect of the purification procedure, we concider an example where each pair initially is in a state given by the density matrix $\hat{\rho}$. We express $\hat{\rho}$ in the Bell basis $\{|\phi^+\rangle, |\psi^-\rangle, |\psi^+\rangle, |\phi^-\rangle\}$ and denote by $\{A, B, C, D\}$ the diagonal elements in the basis. Of particular interest is the element $A = \langle\phi^+|\hat{\rho}|\phi^+\rangle$ which is probability that the qubit pair would pass a test for being in the $|\phi^+\rangle$ state. The aim of the purification protocol is to drive this coefficient to 1 and thus forcing all other entanglement out of the system.

[3]One obtains the same results, as if the flip occurred in the target pair.

When the qubit pair is in the maximally entangled $|\phi^+\rangle$ state, then it cannot be entangled with anything else.

Looking at an hole ensemble of states we can calculate the average diagonal elements after the procedure $\{\tilde{A}, \tilde{B}, \tilde{C}, \tilde{D}\}$. These will, according to [9], have the following dependency on the diagonalelements prior to the procedure,

$$\begin{aligned} \tilde{A} &= \frac{A^2 + B^2}{N} & \tilde{B} &= \frac{2CD}{N} \\ \tilde{C} &= \frac{C^2 + D^2}{N} & \tilde{D} &= \frac{2AB}{N} \end{aligned} \tag{6.11}$$

We have used that $N = (A+B)^2 + (C+D)^2$ is the probability that Alice and Bob obtain coinciding outcomes in their measurements on the target pair.

The figure fig. 6.2 plot the effect of the purification procedure on average, as given in 6.11. It is a plot of the the fidelity as a function of the number of iterations and the initial fidelity. The initial states were prepared with $B = C = D$.

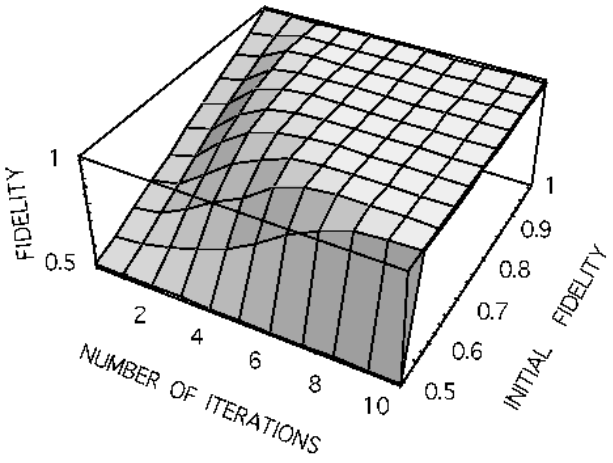

Figure 6.2: *The plot shows the average fidelity of the qubit pairs as a function of initial fidelity and the number of iterations. The initial state is prepared with B=C=D. The figure is from the paper by Deutsch et al. [9].*

An important comment needs to be made on the matter of privacy amplification. The qubit pairs that Alice and Bob receives could have been stolen by an eavesdropper, who we will refer to as evil Eve, she could have entangled the qubits with some qubits of her own. Eve could measure on her own qubits and listen to Alice and Bob talk about their results of the measurement of the targets in the cNOT. Eve is assumed evil, she will do anything in her power to obtain whatever secret message Alice and Bob are exchanging. Now that she has a set of qubits entangled with those shared by Alice and Bob she has

the means to do this.

When driving the system towards a pure state $A \rightarrow 1$ one also destroys all other entanglement that the environment or evil Eve has made with the system. This effect is very useful in quantum cryptography were one try to find ways to avoid Eve's evil doings.

6.3 Continuous variable implementation

The unitary operation performed by Alice and Bob on their qubits given in equation 6.3 and 6.4 is analogous to making a shift of phases on the continuous variables. This is an easy task to implement in both laboratory and in theoretical calculations, a waveplate[4] and a matrix will suffice. A phase shift of θ on, for example, the $\hat{b}$-mode transforms the creation and annihilation operator according to $\hat{b}' = \hat{b}\exp[i\theta]$ and $\hat{b}^{\dagger\prime} = \hat{b}^\dagger \exp[-i\theta]$.

The part where Alice and Bob perform cNOT operations is more difficult to implement. We seek to do it by a set of $50/50$ beamsplitters and by performing homodyne measurements on two of the outgoing modes from the beamsplitters.

The primary reason for using balanced beamsplitters is to physically mix the two states, if the states are not in contact there is no way we can make one of them more entangled. Entanglement cannot be made locally.

We index the two incoming modes of the beamsplitter $\hat{a}$ and $\hat{b}$ and the outgoing $\hat{c}$ and $\hat{d}$ and let these denote the photoncreation operators for each mode, see figure 6.3. We know that a $50/50$-beamsplitter provides the relationship $\hat{c} = 2^{-1/2}(\hat{a} + i\hat{b})$ and $\hat{d} = 2^{-1/2}(\hat{b} + i\hat{a})$ between the different creation operators.

We can use this beamsplitter relations in combination with the definitions of the continuous variable quadrature $\hat{X}$ for the outgoing modes, to find that

$$\hat{X}_c = \frac{1}{\sqrt{2}}\left(\frac{\hat{a}^\dagger + \hat{a}}{\sqrt{2}} - i\frac{\hat{b}^\dagger - \hat{b}}{\sqrt{2}}\right) \qquad \text{and} \qquad \hat{X}_d = \frac{1}{\sqrt{2}}\left(\frac{\hat{b}^\dagger + \hat{b}}{\sqrt{2}} - i\frac{\hat{a}^\dagger - \hat{a}}{\sqrt{2}}\right). \tag{6.12}$$

We wanted to obtain something comparable to the effect of the cNOT which adds the two arguments directly. We can get this kind of behavior if we apply a phase change $\theta = -\pi/2$ on the input mode $\hat{b}$, and a phase change of $\pi/2$ on the outgoing mode $\hat{d}$. Then we find the following relation, relating the quadratures before both phase changes

[4] A waveplate also called a retarder, is an optical device that alters the polarization state of a light wave travelling through it. A wave plate works by shifting the phase of the light wave between two perpendicular polarization components.

and beamsplitter to the quadratures after

$$\hat{X}_c = \frac{1}{\sqrt{2}}\left(\hat{X}_a + \hat{X}_b\right) \qquad \hat{X}_d = \frac{1}{\sqrt{2}}\left(\hat{X}_b - \hat{X}_a\right) \tag{6.13}$$

$$\hat{P}_c = \frac{1}{\sqrt{2}}\left(\hat{P}_a + \hat{P}_b\right) \qquad \hat{P}_d = \frac{1}{\sqrt{2}}\left(\hat{P}_b - \hat{P}_a\right). \tag{6.14}$$

We see now that the action of this beamsplitter is in some ways similar to that of the cNOT, as it forms the sum of the two incoming modes in one mode and the difference in the other.

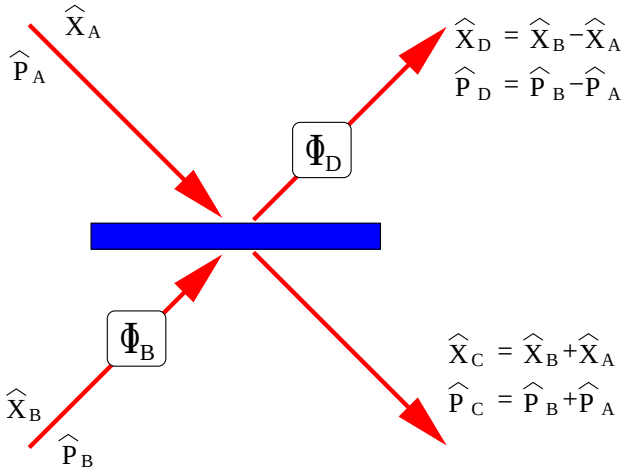

Figure 6.3: *Illustration of the effect of the beamsplitter, with the prober phase shifters introduced, we found them to be* $\phi_B = -\pi/2$ *and* $\phi_D = \pi/2$.

6.3.1 Purification of the TMPS state

We will now examine what effect this could have on the TMPS state. We will use two copies of the TMPS state each of them is prepared in the state

$$|\psi\rangle \approx \frac{1}{\sqrt{2}}(|\hat{X}_{A,+}\hat{X}_{B,+}\rangle + |\hat{X}_{A,-}\hat{X}_{B,-}\rangle). \tag{6.15}$$

We know that if Alice and Bob where to make measurements of their quadratures before the purification procedure they would find

$$\hat{X}_{A1} = \hat{X}_{B1} \qquad \text{and} \qquad \hat{X}_{A2} = \hat{X}_{B2}, \tag{6.16}$$

where 1 and 2 refers to TMPS state 1 and 2.

Now Alice and Bob both measure the quadratures of the outgoing modes from the beamsplitters where the difference between the initial quadratures have been formed. Alice measures $X_A = \hat{X}_{A2} - \hat{X}_{A1}$ and Bob measures $X_B = \hat{X}_{B2} - \hat{X}_{B1}$. Using 6.16 we see that we must have $X_A = X_B$. Just as in the qubit version where we discarded the target and kept the control when Alice and Bob agreed, we will now discard the beamsplitter modes where the difference is formed and keep the beamsplitter modes where the sum is formed when Alice and Bob agree on their measurements.

If Alice and Bob where to do the same measurement when an error is introduced to one of the initial quadratures we get the following calculation:

$$\left\{ \begin{array}{l} \hat{X}_{A1} = \hat{X}_{B1} + \epsilon \\ \hat{X}_{A2} = \hat{X}_{B2} \end{array} \right\} \Longrightarrow \left\{ \begin{array}{l} X_A = \hat{X}_{A2} - \hat{X}_{A1} \\ X_B = \hat{X}_{B2} - \hat{X}_{B1} - \epsilon \end{array} \right\} \Longrightarrow X_A = X_B + \epsilon. \quad (6.17)$$

We see that Alice and Bob will not agree on their measurements when an error is introduced to one of the quadratures. We can therefore use this method to do error finding. Discarding the states where an error has occurred will on average purify the states in an ensemble.

In a quantum mechanical setting, we model this by making a projective measurement of a pair of TMPS states onto the subspace where $X_A = X_B = X_0$.

The resulting joint state formed by the two outgoing beamsplitter modes where no measurement were done, is in an errorfree state and have the same type of correlation $\hat{X}_{res1} = \hat{X}_{res2}$, as there was in each of the incoming states.

6.4 Summary

In this chapter we have presented similarities between, the TMPS state that we found in the previous chapter, and the $|\phi^+\rangle$-Bell state introduced in this chapter. The JP distribution for the TMPS state were seen to exhibit a strong resemblance to the $|\phi^+\rangle$ Bell state.

We found that a measurement of the spin along the z-axis in the spin-$1/2$ representation of the $|\phi^+\rangle$-Bell showed the same correlations as measuring the $\hat{X}$-quadratures in the TMPS state. We found similar correlations for a measurement along the y-axis and a measurement of the $\hat{P}$-quadratures. This enables us to interpret the TMPS state approximately as a continuous variable version of $|\phi^+\rangle$.

We presented details on the purification protocol by Deutsch et al. [9], which work by using beamsplittes and cNOT measurements. This was seen to provide a method for error finding.

Finally we went through steps of making a continuous variable version of the above mentioned purification protocol. The suggested model uses beamsplitters and homodyne measurements, and we have argued that these simple processes should provide a working continuous variable purification protocol. It is important to notice that both the beamsplitter and homodyne measurements are processes that are well mastered in the modern quantum optics laboratory.

The following chapter will provide detailed calculations of the effect of implementing the purification protocol that we developed in this chapter.

Chapter 7

The purified state

This chapter will provide detailed calculations on the purification protocol described in the previous chapter. We calculate the properties of a purified state and use this to evaluate the effect of implementing the protocol. These calculations will to a large extent be carried out using the same kind of manipulations of Wigner functions as we have already seen in chapter 5, where we that presented the TMPS state.

The calculation of the resulting state after the purification protocol will go through three steps. These will be done in the Wigner function formalism, as this behaves nicely under the transformations that we will use. The first step in the purification protocol is a change of phase, this is followed by mixing the outputs on $50/50$-beamsplitters. Thirdly, conditional homodyne measurement of one of the outgoing quadratures from each beamsplitter is performed.

In figure 7.1 a sketch demonstrating the basic features of the proposed setup is presented. Homodyne detection is abbreviated H.D.

The the modes of the two TMPS states are denoted A, B, E and F. The old association of C and D to the vacuum modes have been kept as to not impose unnecessary confusion, the vacuum modes of the other TMPS state are denoted G and H. The nomenclature regarding the modes after phases and beamsplitters are applied are presented later in the chapter.

The change of phase, denoted by the red circles on the schematic drawing, is done on each mode separately and no combined[1] state is thus needed yet. We will however introduce the combined state at this point, as it will prove to make later calculations easier.

[1] Combined is referring to the product of the two TMPS states involved in the protocol.

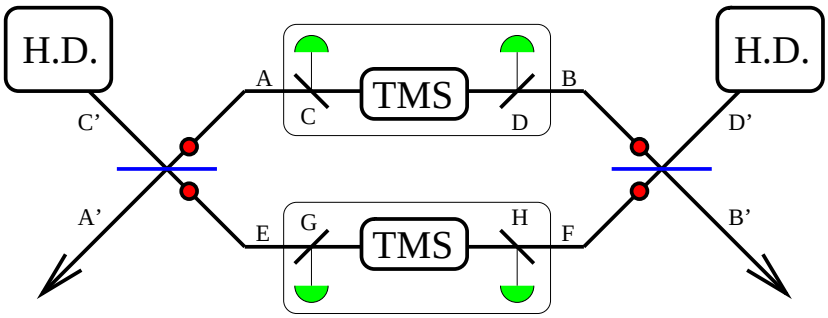

Figure 7.1: *This figure presents an schematic outline of the purification procedure. Two TMPS states are mixed on balanced beamsplitters and two of the outgoing modes are conditionally prepared, the conditioning is due to the result of two homodyne detections. TMS refers to the two mode squeezed state, the framed parts of the sketch contains the TMPS state productions.*

7.1 Wignerfunction of the combined state

The Wigner function of the combined state is simply the product of the Wigner functions for two TMPS states. The small *c* in the subscript refers to conditionally prepared.

$$W_{c,ABEF} = W_{c,AB} \times W_{c,EF} \tag{7.1}$$

We define the vectors, $r_{AB} = [X_A, P_A, X_B, P_B]^T$ and $r_{EF} = [X_E, P_E, X_F, P_F]^T$. Assuming identical setups for the two TMPS states, we can write the combined state as

$$W_{c,ABEF} = \frac{1}{\pi^4 P_G^2 \det \gamma_{out}} \sum_{j=1}^{4} \sum_{k=1}^{4} \frac{q_j q_k}{\sqrt{\det \Gamma_{j,CD} \det \Gamma_{k,GH}}} \times \exp[-(r_{AB}^T \Gamma_{j,AB} r_{AB} + r_{EF}^T \Gamma_{k,EF} r_{EF})] \tag{7.2}$$

where G and H refer to vacuum modes of one system as do C and D to the other, see figure 7.1. The terms $\Gamma_{k,GH}$ and $\Gamma_{k,EF}$ are analogous to $\Gamma_{j,CD}$ and $\Gamma_{j,AB}$ which we encountered when calculating the TMPS state. The combined state can be rewritten with the introduction of the $R = r_{AB} \oplus r_{EF}$ and the $[8 \times 8]$ matrix

$$\Gamma_{j,k} = \begin{bmatrix} \Gamma_{j,AB} & 0 \\ 0 & \Gamma_{k,EF} \end{bmatrix}. \tag{7.3}$$

This simplifies the expression to some degree.

$$W_{c,ABEF} = \frac{1}{\pi^4 P_G^2 \det \gamma_{out}} \sum_{j=1}^{4} \sum_{k=1}^{4} \frac{q_j q_k}{\sqrt{\det \Gamma_{j,CD} \det \Gamma_{k,GH}}} \exp[-R^T \Gamma_{j,k} R)] \quad (7.4)$$

It is now an easy task to apply the change of phase, we have seen in a previous chapter that this operation is modelled simply by a matrix being multiplied onto the $\Gamma_{j,k}$ matrix.

$$\Gamma_{j,k} \rightarrow S\, \Gamma_{j,k}\, S^T \quad (7.5)$$

Generally we know that a Wigner function of a state after a linear operation S can easily be calculated. For a linear transformation $R' = SR$ we find that the following relation between the final and incoming Wigner functions is true

$$W_{final} = W_{incoming}(S^{-1}R). \quad (7.6)$$

The proof of this is straightforward.

7.2 Change of phase and 50/50-beamsplitter

The combined phase change matrix is a direct sum of the phase change matrices over each of the four modes (A,B,E,F), forming a matrix of dimensions [8×8],

$$S_{PH,\Delta} = \begin{bmatrix} \cos\theta_A & \sin\theta_A \\ -\sin\theta_A & \cos\theta_A \end{bmatrix} \oplus \cdots \oplus \begin{bmatrix} \cos\theta_F & \sin\theta_F \\ -\sin\theta_F & \cos\theta_F \end{bmatrix}. \quad (7.7)$$

This is the first step in the purification protocol. We will wait with the multiplication on the covariance matrix as given in 7.5, because more matrices will have to be applied and we might as well wait and do them all at once.

The second step in the purification protocol consists of mixing of the incoming modes on a set of balanced beamsplitters. In the previous chapter we found that we could build a beamsplitter that performed in a controlled way on the incoming quadratures. The beamsplitter imposes a set of relationships between the quadratures of the incoming and outgoing modes,

$$\hat{X}_{A'} = \frac{1}{\sqrt{2}}(\hat{X}_A + \hat{X}_E) \qquad \hat{P}_{A'} = \frac{1}{\sqrt{2}}(\hat{P}_A + \hat{P}_F) \quad (7.8)$$

$$\hat{X}_{C'} = \frac{1}{\sqrt{2}}(\hat{X}_E - \hat{X}_A) \qquad \hat{P}_{C'} = \frac{1}{\sqrt{2}}(\hat{P}_E - \hat{P}_A) \quad (7.9)$$

and in a similar way for B', D', B and F. These kind of transformations are easy to express in matrix form, here we will denote the balanced beamsplitting matrix S_{BBS}. Using the identity 7.6 we define $R' = [X_{A'}, X_{B'}, P_{A'}, P_{B'}, X_{C'}, X_{D'}, P_{C'}, P_{D'}]^T$. The linear transformation that takes R to R' is partly due to S_{BBS} and partly to a homogeneous matrix $S_{hom'}$ that reorders the rows in the matrix in a way that will prove advantageous, $R' = S_{hom'}\ S_{BBS}\ R$. Both S_{BBS} and $S_{hom'}$ are easy to calculate from the above equations.

from 7.8 and the wanted form of R', we will therefore not include the huge $[8 \times 8]$ matrices here.

Implementing the first and the second step of the purification protocol plus a reordering of the rows, that we will use when we do homodyne detection, amounts to doing matrix multiplication. We need to do the following transformation

$$\Gamma'_{j,k} = S_{hom'} S_{BBS} S_{PH,\Delta} \Gamma_{j,k} S^T_{PH,\Delta} S^T_{BBS} S^T_{hom'} \tag{7.10}$$

which we will use in

$$W_{A'B'C'D'} = \frac{1}{\pi^4 P_G^2 \det \gamma_{out}} \sum_{j=1}^{4} \sum_{k=1}^{4} \frac{q_j q_k}{\sqrt{\det \Gamma_{j,CD} \det \Gamma_{k,GH}}} \exp[-R'^T \Gamma'_{j,k} R')] \tag{7.11}$$

The Wigner function presented above, now describes the joint state immediately before the lightbeams impinge on the homodyne detectors. The Wigner function is now dependent on the quadratures in the four modes A', B', C' and D'.

7.3 Homodyne measurements

The third step of the protocol is a set of homodyne measurements of the quadratures where we condition on finding the same result, the measurements are done in modes C' and D'. We will denote the measurementgoal for the homodyne measurements X_0 and treat this as an variable in our model. The conditioning is modelled by making a projection of the Wigner function unto a state with $|\hat{X} = X_0\rangle$.

From the background theory chapter we know how to calculate the density operator for the joint state after the homodyne projections. It can be found as a partial trace of the product of the projection operator and the density operator for the entire joint state,

$$\hat{\rho}_{HD,A'B'} = \mathrm{Tr}_{C'D'} \left[|X_{0,C'}\rangle |X_{0,D'}\rangle \langle X_{0,D'}| \langle X_{0,C'}| \hat{\rho}_{A',B',C',D'} \right]. \tag{7.12}$$

The partial trace can be calculated using the identity 4.14 found in the chapter on Wigner functions, we thus only need to perform the following calculation.

$$\hat{\rho}_{HD,A'B'} = (2\pi)^2 \int dX_{C'} dP_{C'} dX_{D'} dP_{D'}\, W_{\hat{proj}}(\hat{R}')\, W_{\hat{\rho}_{A',B',C',D'}}(\hat{R}') \tag{7.13}$$

We use that $\hat{R}' = [\hat{X}_A, \hat{X}_B, \hat{P}_A, \hat{P}_B, X_C, X_D, P_C, P_D]^T$, because the Wigner functions are defined for modes C and D only. We know from [25] that the quadrature operators can be replaced with numbers when calculating the Wigner function of a Gaussian density operator.

This expression contains two Wigner functions. Both Wigner functions are defined for the modes C and D but the expression should still be considered quantum operators for the modes A and B. The Wigner function of $\hat{\rho}_{A',B',C',D'}$ takes the form of 7.11 and is denoted $W_{A'B'C'D'}(\hat{R}')$, the hat on R reminds us that it is not just a function.

The Wigner function of the projection operators is given as the product of the following expression for modes C' and D',

$$\begin{aligned} W_{\hat{proj},C'} &= \frac{1}{\sqrt{2\pi}} \int dx'\, \langle X_{C'} - x'/2 | X_{0,C'} \rangle \langle X_{0,C'} | X_{C'} + x'/2 \rangle \exp[iP_{C'}x'] \\ &= \frac{1}{\sqrt{2\pi}} \int dx'\, \delta(X_{C'} - x'/2 - X_{0,C'}) \delta(X_{C'} + x'/2 - X_{0,C'}) \exp[iP_{C'}x'] \\ &= \frac{1}{\sqrt{2\pi}} \int dx'\, \delta(x') \delta(X_{C'} - X_{0,C'}) \exp[iP_{C'}x'] \\ &= \frac{\delta(X_{C'} - X_{0,C'})}{\sqrt{2\pi}} \end{aligned} \tag{7.14}$$

The calculation of $\hat{\rho}_{HD,A'B'}$ is now reduced to doing the integral

$$\begin{aligned} \hat{\rho}_{HD,A'B'} &= 2\pi \int dX_{C'} dP_{C'} dX_{D'} dP_{D'}\, \delta(X_{C'} - X_0) \delta(X_{D'} - X_0) W_{A',B',C',D'}(\hat{R}') \\ &= 2\pi \int dP_{C'} dP_{D'}\, W_{A',B',C',D'}(\hat{R}') \Big|_{X_{C'} = X_{D'} = X_0} \end{aligned} \tag{7.15}$$

The Wigner function of the state in modes A' and B' after we have done the homodyne projections can now be calculated as

$$\begin{aligned} \tilde{W}_{HD,A',B'} = \frac{1}{(2\pi)^2} \int dx' dx'' \langle X_{A'} - x'/2 | \langle X_{B'} - x''/2 | \hat{\rho}_{HD,A'B'} \\ \times | X_{B'} + x''/2 \rangle | X_{A'} + x'/2 \rangle \exp[i(P_{A'}x' + P_{B'}x'')] \end{aligned} \tag{7.16}$$

Just as when we calculated the Wigner function for the TMPS state, can we now replace

the quadrature operators with numbers. We can therefore treat $\hat{\rho}_{HD,A',B'}$ as a constant which make the expression easy to evaluate. We find that

$$\tilde{W}_{HD,A',B'} = \frac{1}{2\pi}\int dP_{C'}dP_{D'}\, W_{A',B',C',D'}(R')\Big|_{X_{C'}=X_{D'}=X_0}. \tag{7.17}$$

This integration is easily done using Appendix A. The purpose of $S_{hom'}$, was to rearrange the quadratures in such a way that the the integral above has the form used in this appendix.

Using Appendix A we have to divide the $\Gamma'_{j,k}$ into submatrices in the following way:

$$\Gamma'_{j,k} = \begin{bmatrix} A'_{j,k}[6x6] & C'_{j,k}[6x2] \\ C'^{T}_{j,k}[2x6] & B'_{j,k}[2x2] \end{bmatrix} \tag{7.18}$$

We define a new vector $R'_{HD} = [X_{A'}, X_{B'}, P_{A'}, P_{B'}, X_0, X_0]^T$ and a new set of matrices $\Gamma'_{HD,j,k} = A'_{j,k} - C'_{j,k}B'^{-1}_{j,k}C'^{T}_{j,k}$, using the submatrices. Using all this, we finally find that the Wigner function of the state after the homodyne projection have been made, is given by

$$\tilde{W}_{HD,A',B'} = \frac{1}{2\pi^4 P_G^2 \det\gamma_{out}}\sum_{j=1}^{4}\sum_{k=1}^{4}\frac{q_j q_k \exp[-R'^{T}_{HD}\Gamma'_{HD,j,k}R'_{HD}]}{\sqrt{\det\Gamma_{j,CD}\det\Gamma_{k,GH}\det B'_{j,k}}}. \tag{7.19}$$

The resulting Wigner function is unnormalized, which we have indicated by a $\sim$ on top of the W. Before we can start quantifying the correlations we need to normalize the Wigner function.

7.3.1 Normalization

We see that the Wigner function is a sum of 16 gaussian functions, and is given in the equation above. The normalization is done by integrating the Wigner function 7.19 up over the entire phase space, which is given by the modes A' and B',

$$\int dX_A dX_B dP_A dP_B\, \tilde{W}_{HD,A',B'}. \tag{7.20}$$

The result can thus be used to express the normalized Wigner function as

$$W_{HD,A',B'} = \frac{1}{\pi^2 P_H}\sum_{j=1}^{4}\sum_{k=1}^{4}\frac{q_j q_k \exp[-R'^{T}_{HD}\Gamma'_{HD,j,k}R'_{HD}]}{\sqrt{\det\Gamma_{j,CD}\det\Gamma_{k,GH}\det B'_{j,k}}} \tag{7.21}$$

To do the aforementioned integral we once more need to reorder the terms in the exponential function by a matrix $S_{hom''}$ to form the new ordering given as

$$R''_{HD} = [X_0, X_0, X_{A'}, X_{B'}, P_{A'}, P_{B'}]^T. \tag{7.22}$$

Splitting the matrices $\Gamma'_{HD,j,k}$ into a set of smaller matrices in the following way,

$$S_{hom''}\Gamma'_{HD,j,k}S^T_{hom''} = \begin{bmatrix} A'_{HD,j,k}[2x2] & C'_{HD,j,k}[2x4] \\ C'^T_{HD,j,k}[4x2] & B'_{HD,j,k}[4x4] \end{bmatrix} \tag{7.23}$$

enables us to find

$$P_H = \sum_{j=1}^{4}\sum_{k=1}^{4} \frac{q_j q_k \exp[-[X_0, X_0](A'_{HD,j,k} - C'_{HD,j,k}B'^{-1}_{HD,j,k}C'^T_{HD,j,k})[X_0, X_0]^T]}{\sqrt{\det\Gamma_{j,CD}\det\Gamma_{k,GH}\det B'_{j,k}\det B'_{HD,j,k}}} \tag{7.24}$$

The normalized Wigner function can now be used to find the JP distribution for measurements of the quadratures in the A' and B' modes. The coefficient P_H is related to the probability of measuring X_0 in the C' and D' modes, and thus conditionally preparing the state, we will take briefly on this probability later.

7.4 Calculation of the JP distribution

We follow much the same scheme as we did for the TMPS state, but with the addition of the conditional homodyne detection. The added conditional homodyne detection causes the matrices describing the system to have dimension $[6 \times 6]$ to be compared with $[4 \times 4]$ needed by the TMPS state. This complicate the expressions a bit.

We perform the calculation

$$P(X_{A,\theta_j}, X_{B,\phi_k}) = \int dP_{A,\theta_j} dP_{B,\phi_k}\, W_{HD,A,B}(S^T_{sh,jk,HD}R''_{HD}), \tag{7.25}$$

where A' and B' have now been substituted with simply A and B. The matrices $S_{sh,jk,HD}$ are phase change matrices defined in the same manner as previously 5.31, with the addition of an identity matrix for the X_0 rows.

We use $S_{hom''}$ as given above to reorder the rows, and multiply with the phase change matrix. We the divide the resulting matrices into a set of smaller matrices

$$S_{sh,jk,HD}S_{hom''}\Gamma'_{HD,j,k}S^T_{hom''}S^T_{sh,jk,HD} = \begin{bmatrix} A''_{HD,j,k}[4x4] & C''_{HD,j,k}[4x2] \\ C''^T_{HD,j,k}[2x4] & B''_{HD,j,k}[2x2] \end{bmatrix} \tag{7.26}$$

We define $r = [X_0, X_0, \hat{X}_A, \hat{X}_B]^T$ along with

$$\Gamma''_{HD,j,k} = A''_{HD,j,k} - C''_{HD,j,k} B''^{-1}_{HD,j,k} C''^{T}_{HD,j,k} \tag{7.27}$$

and we find the JP distribution to be

$$P_{HD,A,B} = \frac{1}{\pi P_H} \sum_{j=1}^{4} \sum_{k=1}^{4} \frac{q_j q_k \exp[-r^T \Gamma''_{HD,j,k} r]}{\sqrt{\det \Gamma_{j,CD} \det \Gamma_{k,GH} \det B'_{j,k} \det B''_{j,k}}} \tag{7.28}$$

The joint probability function is now a function of X_A, X_B and X_0.

The dependency on X_0 causes the function to be asymmetric, which make the calculation of the correlation coefficients somewhat more complicated.

7.5 Correlation coefficients

When calculating the correlation coefficients of the TMPS state, we used that the JP distribution was symmetric and normalized, thus reducing the 4 integrals to 1. The JP distribution describing the purified is still normalized, but the conditioning on a homodyne detection has left the state asymmetric. We need to do the integral

$$E(\theta_j, \phi_k) = \int dX_{A,\theta_j} dX_{B,\phi_k} \operatorname{sign}\left(X_{A,\theta_j} X_{B,\phi_k}\right) P_{HD,A,B}(X_{A,\theta_j}, X_{B,\phi_k}) \tag{7.29}$$

The problem is how to integrate the exponential function $\exp[-r^T \Gamma''_{HD,j,k} r]$ with $r = [X_0, X_0, \hat{X}_A, \hat{X}_B]^T$. We do the first integral, the integral over X_{A,θ_j}, analyticly and the second numerically. Firstly, we rewrite the exponential function to have the form

$$\begin{aligned} \exp[-r^T \Gamma''_{HD,j,k} r] = \exp[&\alpha_1 X^2_{A,\theta_j} + \alpha_2 X^2_{B,\phi_k} + \\ &+ \alpha_3 X_{A,\theta_j} X_{B,\phi_k} + \alpha_4 X_{A,\theta_j} + \alpha_5 X_{B,\phi_k} + \alpha_6] \end{aligned} \tag{7.30}$$

To find the different α_n we divide $\Gamma''_{HD,j,k}$ in four smaller matrices given by

$$\Gamma''_{HD,j,k} = \begin{bmatrix} \Delta_A[2x2] & \Delta_C[2x2] \\ \Delta_C^T[2x2] & \Delta_B[2x2] \end{bmatrix} \tag{7.31}$$

which again are divided as

$$\Delta_C = \begin{bmatrix} c_{11} & c_{12} \\ c_{21} & c_{22} \end{bmatrix} \qquad \text{and} \qquad \Delta_B = \begin{bmatrix} b_{11} & b_{12} \\ b_{21} & b_{22} \end{bmatrix} \tag{7.32}$$

We know that $\Gamma''_{HD,j,k}$ is a symmetric matrix, so $b_{12} = b_{21}$. With these definition the α-coefficients are given as

$$\begin{aligned} \alpha_1 = -b_{11}, \quad \alpha_2 = -b_{22}, \quad \alpha_3 = -2b_{12}, \quad \alpha_4 = -2(c_{11} + c_{21})X_0, \\ \alpha_5 = -2(c_{12} + c_{22})X_0, \quad \text{and} \quad \alpha_6 = -[X_0, X_0]\Delta_A[X_0, X_0]^T \end{aligned} \tag{7.33}$$

The integrations from $-\infty \ldots \infty$ for each of the two quadratures in 7.29 are split up in semi infinite intervals, which allows for an easy evaluation of the sign function. Generally we can rewrite an integral in the following way: $\int_{-\infty}^{0} f(x)dx = \int_{0}^{\infty} f(-x)dx$, using this property we will only have to calculate integrals of the form $\int_0^\infty f(\pm x)dx$, when evaluating 7.29.

Setting $b = \alpha_3 X_{B,\phi_k} + \alpha_4$ and $c = \alpha_2 X^2_{B,\phi_k} + \alpha_5 X_{B,\phi_k} + \alpha_6$, and use that $\alpha_1 < 0$ we find that

$$\int_0^\infty dX_{A,\theta_j} \exp[-r^T \Gamma''_{HD,j,k} r] = \frac{\sqrt{\pi}}{2\sqrt{-\alpha_1}} \exp\left[-\frac{b^2}{4\alpha_1} + c\right] \operatorname{Erfc}\left[-\frac{b}{2\sqrt{-\alpha_1}}\right] \tag{7.34}$$

Where $\operatorname{Erfc}[x] = 1 - \operatorname{Erf}[x]$ is the complimentary errorfunction. The errorfunction is defined as $\operatorname{Erf}[x] = \frac{2}{\sqrt{\pi}} \int_0^x dt \exp[-t^2]$.

The integration over X_B in 7.34 is too complicated to be done analytically so we do the integration numerically[2]. Having done this, we form the correlation coefficient as the sum over 4 integrals, one from each quadrant in the $X_{A,\theta_j}, X_{B,\phi_k}$ coordinate system.

If we were to condition on $X_0 = 0$, then the above calculations would simplify a great deal. We could then use the same algebraic step as we used when we calculated the correlation coefficients for the TMPS state, thus avoiding numerical integrations.

7.6 Results

To calculate the Bell parameter we take must choose 2 sets of angles for calculation of the 4 coorelation coefficients.

$$S_{Bell} = |E(\theta_1, \phi_1) + E(\theta_1, \phi_2) + E(\theta_2, \phi_1) - E(\theta_2, \phi_2)| \tag{7.35}$$

Optimizing the angles trying to achieve the highest Bell parameter, we find $\theta_1 = \pi/2$, $\theta_2 = \pi$, $\phi_1 = -\pi/4$ and $\pi/4$. These values are almost the same values as for the TMPS state. The JP distributions associated with each of the four coorelation coefficients are also, one for one almost identical to those we found for the TMPS state.

[2]These calculations are done using Mathematica.

We see in figure 7.2 that the JP distribution, where the correlation coefficient is associated with a minus in the Bell parameter, exhibit the opposite correlation when compared to the others. This is a feature shared with the TMPS state.

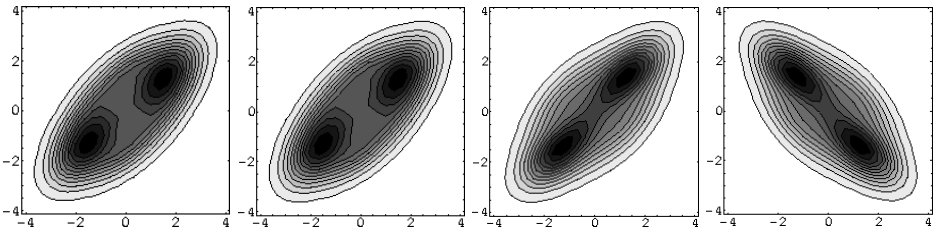

Figure 7.2: *Plot of the four probability distributions for the choice of angles that led to a maximum violation of Bell's inequality after the application of the purification protocol. The two axes are X_A and X_B respectively. The optimal phases applied to the four modes where found to be $\theta_A = -\pi/2$, $\theta_B = 0$, $\theta_E = -\pi/2$ and $\theta_F = 0$. The homodyne measurement phases are $(\theta, \phi) = \{(\pi/2, -\pi/4), (\pi/2, \pi/4), (\pi, -\pi/4), (\pi, \pi/4)\}$.*

The plots of the JP distribution shown in figure 7.2 are all shown for $X_0 = 0$. The reason for this is that $X_0 = 0$ is the optimal choice, as we will show below.

7.6.1 Optimization of the homodyne projection

We have done many simulations varying all the different parameters and found that the best results were achieved for $X_0 = 0$. The dependency on X_0 is a seen to be similar to a Gaussian bell with peak around 0. Below is a plot of this dependency, shown for the purified state with the highest Bell parameter (found for $\lambda = 0.508$).

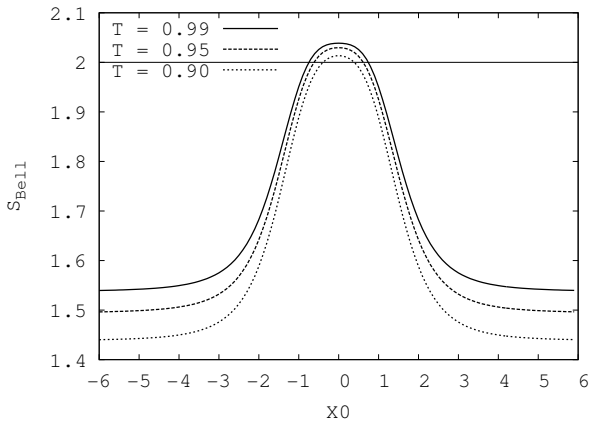

Figure 7.3: *The dependency on X0 is plotted for the three different values of T, it is clear that the optimal choice is $X_0 = 0$.*

The reason that zero is the best choice for the homodyne conditional measurement, is due to the properties of the states we mix on the 50/50-beamsplitter. We mix two copies of the same state that exhibit a high probability of having similar quadratures $X_{A,n} = X_{B,n}$. But as the states are alike then we also with a high probability find $X_{A,1} = X_{A,2}$ and $X_{B,1} = X_{B,2}$. If an error ϵ have been introduced, then we find the result of the outgoing mode to be $X_{A,1} - X_{A,2} + \epsilon = \epsilon$, so conditioning on this measurement equal to zero forces us to disregard the states with an error present.

7.6.2 Dependency on squeezing

Below, see figure 7.4, we plot how the Bell-parameter depends on the amount of squeezing applied to the initial state. The figure features three different degrees of transmitivity of the beamsplitters, that now are responsable for 4 photon subtractions, two for each TMPS state. This is a plot similar to what we showed for the two photon subtracted state.

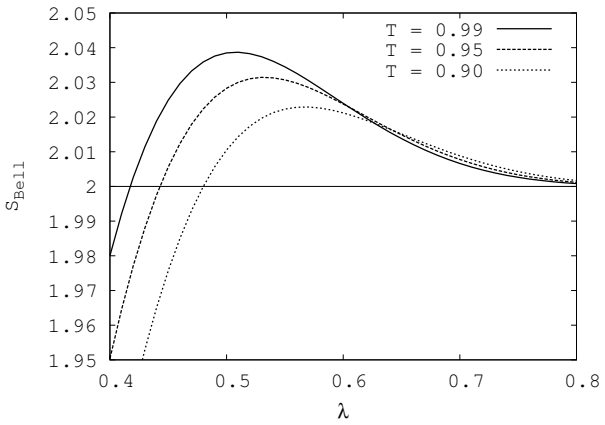

Figure 7.4: *Plot of the dependency on the squeezing λ for three different levels of transmittance on the photon subtracting beamsplitters, for the purified state. We see violation of Bell in the percent range and see the peaks shifted towards lower squeezing as compared to the TMPS state.*

We can see that this plot have all the same features as the corresponding plot for the two photon subtracted state. The main difference between the two plots is that the peaks of the later purified state are shifted towards a lower degree of squeezing and peaks at a slightly lower value.

7.6.3 Comparing to the TMPS state

We want to see how the states after purification compare to the states before the purification. We plot this separately[3] for the three values of T that we have used throughout this project. The plot for T = 0.99 is shown in figure 7.5 below.

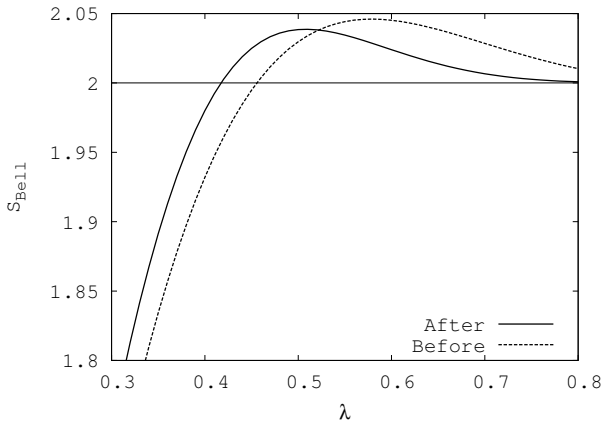

Figure 7.5: *Plot of the effect on the purification protocol. The results shown are for T = 0.99 and X_0=0. We see that the protocol works for low values of squeezing.*

We can see from figure 7.5 that we will not be able to give a simple "yes/no"-style answer to the question: "does it work?".

On one side we can argue that the purification protocol is not a complete success, as it fails to produce a higher violation of Bell's inequality than what we already had from the TMPS state. But on the other side we see that for a large interval of squeezing values, we find that the Bell-parameter is being increased a significant amount. We could argue that the purification protocol does work, except for a state that is already too close to optimal.

We plot the result of the purification protocol for the interval of squeezing where we find that the purification protocol works, see figure 7.6. The results are most prominent for a high value of T (T=0.99), this is the value used in the plot below.

Especially it is worth noticing that for $\lambda \in [0.418 : 0.456]$ we see that the purification protocol takes a state from $S_{Bell} < 2$ to $S_{Bell} > 2$. This feature clearly proves that the suggested purification protocol conceptionally works.

[3]The plot below is for T = 0.99, for the two other values of T we refer to appendix C.

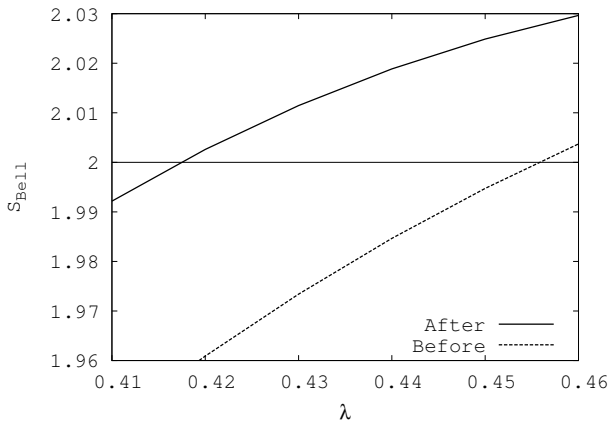

Figure 7.6: *Plot of the effect on the purification protocol. The results are shown for T = 0.99 and $X_0 = 0$. The plot shows a slice of figure 7.5, focusing on an interval of squeezing where the purification process take a state that before were unable to break Bell's inequality to a state that is able to break Bell.*

7.6.4 Perfect detectors

In the calculations on the purified state we have not included the effect of imperfect detectors, the reason for this is twofold.

Firstly. We saw from the TMPS state that the inclusion of imperfect initial photodetectors had very little influence on the achievable Bell values. We can experimentally perform the homodyne detections with a efficiency so high, that a model of a imperfect realistic measurement ($\eta_{HD} \approx 0.95$) is very close to a model where perfect homodyne detection are used. The results obtained from realistic values are thus close to what we obtain using perfect detection.

Secondly. A study of these small effects would have been considered a subject of greater importance, had the results of the suggested protocol been more favorable. The aim of this thesis will be to find results for the optimal choice of values, not how they depend on imperfections.

For these reasons we will always use perfect detectors when we model their effects on the purified state.

7.7 Repeating the protocol

The natural next steps is to do the hole thing again, this time using the purified states as input instead of the TMPS states. This iterative process could go on forewer, but due to

timeconstraints and lack of computational power we will only calculate the result for one more iteration.

The calculations are similar to what we have already done. The main difference is that all the expressions involved grow from involving 16 terms to $16^2 = 256$ terms. We choose to condition on $X_0 = 0$ as this was found to be the optimal value. Using this conditioning all the calculations are reduced to linear algebra and a few wellknown analytical functions.

The purification protocol did not produce a overall higher Bell parameter when it was applied the first time to the TMPS state. We do therefore not expect to see an increase applying it a second time. One could suspect though, that there will be a interval of the squeezing parameter were the purification protocol take states with a lower Bell value to a state with a higher Bell value.

7.7.1 Outline of the calculations

We will have to go through all the same calculations as already presented in this chapter in order to do a second iteration of the purification procedure. We will therefore only present a outline of the calculations.

We first need to construct the joint state describing the unification of two copies of the purified state. The Wigner function of the joint state W_{2nd} is found to be

$$W_{2nd} = W_{HD,A',B'} \times W_{HD,X',Y'} \tag{7.36}$$

Each of the Wigner functions for the purified states consists of a sum of 16 terms, the combined Wigner functions therefore grows to contain 256 terms. Each term in the combined Wigner function is manipulated in the same manner as we have done when we were applying the protocol the first time.

Going through the somewhat sizable number of terms expressing the different properties of the state, we find that the Wigner function of the two times purified state takes the form.

$$W_{2nd} = N \sum_{i=1}^{4} \sum_{j=1}^{4} \sum_{k=1}^{4} \sum_{l=1}^{4} C_{ijkl} \exp[-r^T \Gamma_{ijkl} r] \tag{7.37}$$

with $r = [X_A, P_A, X_B, P_B]^T$. The exact form of N, C_{ijkl} and Γ_{ijkl} can be found going through all the same steps as with the first iteration of the protocol. The calculations will not be presented here as we will not learn anything new from them, we will however present the results.

For an optimal choice of angles the two time purified state has the following depen-

dence on the squeezing for three different values of T. We see again that the shape of this plot is very similar two what we previously found for both the TMPS and one time purified state.

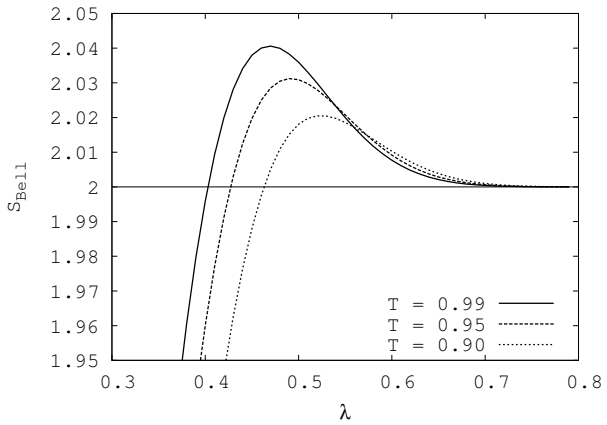

Figure 7.7: *This plot contains the results for the two time purified state, it shows the dependency of the squeezing for an optimal choice of angles, plotted for three different values of T. Again we see violation of Bell in the percent range and find that the optimal squeezing value is lower than for both the one time purified state and the TMPS state.*

We plot the Bell parameter as a function of squeezing for a fixed value of T for the TMPS, the once purified and the time purified state, see figure 7.8 to the left. We see a tendency towards finding the optimal result for a lower and lower squeezing.

We enlarge a section of this plot, focussing on the range of squeezing where we can see that the purification protocol works, see figure 7.8 to the right. We see that for a given amount of squeezing the purification protocol can take the Bell parameter from approximately 1.98 over 2.015 to 2.03, exactly as wanted.

We can see from figure 7.8 that the value of the optimal squeezing is lowered after each step of the purification protocol. We also see that we were wrong when we thought that the peak of the two time purified state would be situated lower than the peak of the one time purified state. As would be suspected from solely seing the result of one purification procedure.

Due to time constraints it has not been possible to undertake an investigation of this surprising feature in this thesis.

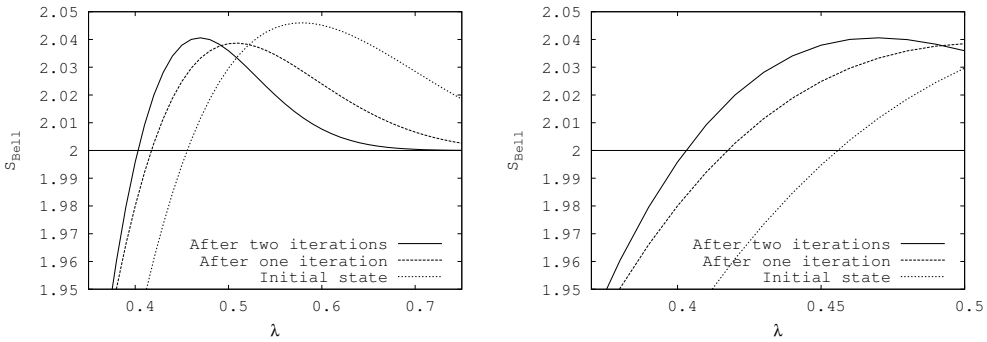

Figure 7.8: *Dependency of the squeezing for an optimal choice of angles, plotted for the initial state, the state after one iteration and after two iterations. All three plots for T = 0.99.. The plot on the right shows a section where the protocol is seen to be particularly effectfull. It is surprising to see that the two time purified state peaks higher than the purified state, it would be interesting to see if this tendency would continue in a third iteration.*

7.8 Probability of success

When we do conditional homodyne projection and subtraction of the photons, we associated a probability of success to the processes. Success meaning that we accomplished what we sat out to do, that is, finding X_0 in the homodyne measurement and observing a click in the avalanche photo-detector.

Let us first look at the photon subtraction. When we let the transmitivity of the mirrors that subtracting a photon go towards one ($T \to 1$) we are less and less likely to observe a click in the photodetectors. The normalizing number P_G done in the calculations for the TMPS state is the probability for seeing a click in both detectors. We saw in the chapter on the TMPS state that the probability for a successfull generation of a TMPS state is smaller than $1/1000$ in the case of T = 0.99, for a interesting value of squeezing.

The trouble with this is that when we use the purification protocol we need to mix sets of these states. The probability of a simultaneous generation of two TMPS states is found as the square of the probability for one, which is denoted P_G. The result is that the corresponding probability of success drops to a point where it is close to infeasible to do the experiments.

If we had a way of saving the TMPS states, we could avoid this problem. A quantum memory for light could help fix this problem, we could save the first conditionally prepared state until we had another and then let them interact.

We also associate a probability of success to the homodyne projective measurement on $X_0 = 0$. We have allready calculated the normalization coefficient associated with the

homodyne projection P_H. The probability density of a successfull homodyne projection is related to P_H through

$$P_{succes,HD} \propto \frac{P_H}{P_G^2 \det[\gamma_{out}]} \tag{7.38}$$

This can be seen from the relationship between the unnormalized and normalized Wigner functions for the purified state. I have plotted $P_{succes,HD}$ as a function of X_0 and seen that we achieve the highest probability for $X_0 = 0$, the plot is not included shown in this thesis.

We do not condition on a interval of quadrature phases. This leaves the probability of success equal to zero, as a projection to exactly $X_0 = 0$ has an infinitesimal probability. The dependence on conditioning on a small interval of quadratures should be calculated before setting out to do an experimental test of the proposed setup.

7.9 Method

In the Mathematica programs we calculate the Bell parameter for different choices of values of the phase space. The program can be configuered to change each parameter a small amount for each calculation of the Bell parameter. The calculation of the Bell parameter is placed within a set of FOR loops and we have tried to be very careful to examine the entire phase space for optimal values of all the parameters.

This method offers no garantie that what we have found is optimal, but we feel confident that the values for the choice of phases are optimal even though the phase space is huge. It is possible to vary 8 different phases plus the value for X_0.

7.10 Previous research in continuous variable purification protocols

In this section we will give a outline the work closely related to this thesis, that is being done in other research groups around the world.

We have seen that there exists a interval of squeezing where the purification protocol suggested in this thesis definitely works. Even though the results are not overwhelming the protocol seem to have the desired effect. There are though other ways of preparing a continuous variable state that is capable of breaking Bells inequality.

Sonja Daffer and Peter L. knight

Let us start by making a outline the results of found by Sonja Daffer and Peter L. Knight [33]; they generate near optimal states for use in a homodyne Bell test. Their protocol take a pair of two-mode squeezed states and mix them pairwise on a unbalanced beamsplitter. Two of the outgoing modes are subjected to a photo-detector that differentiate between the absence and presence of photons only. This first step has some of the same features as the preparation process presented earlier in this thesis, but here they firstly mix a pair of two mode squeezed states and then subtract a photon.

The second step of their protocol, which they repeat three times, is to combine two of the outgoing beams that have not had a photon subtracted, on balanced beamsplitters and then measure with a photo-detector on one of the outgoing modes. If no photon is detected, then the state is kept to be used in the next iteration, a total of three iterations are performed.

Before making the final homodyne Bell measurement a photon is subtracted from each mode. This is done in the same way as we have presented earlier, that is, by mixing each mode with vacuum on an unbalanced beamsplitter and detecting a click in the photodetector.

Their results are impressive, they get very near to the optimal Bell parameter. They achieve $S_{Bell} = 2.071$ as compared to the highest possible value[4] $S_{Bell} = 2.076$, there is a problem however. In the iterative procedure they have conditioned on seeing their photodetector perform a "no-click". Conditioning on not observing a click is not a good property, especially if one were to try to realize an experimental setup.

García-Patrón, R. et al.

One of the groups of authors that presented the TMPS state as a candidate for an experimental realization of an loophole-free Bell inequality test [8], also elaborated in a later and more thourough paper [31] on different ways to achieve a higher Bell violation.

They [31] consider different setups varying the incoming states (single mode squeezing in either the X or P direction), the use of balanced beamsplitters and the number and placement of single photon subtractors. Their results are striking, they find find it impossible to break Bell's inequality for an odd number of photon subtractions, this results is not a general statement but they found it to be true for all the cases they considered.

They further found that the scheme presented as the TMPS state is seen to be the produced from the best configuration where two photons have been subtracted, at least

[4]This is the highest violation of Bells inequality with a state of the form $|\psi\rangle = \sum_n C_n|n,n\rangle$. Our protocol implements a conditional homodyne detection, thus leaving this photon number coupled regime.

when it comes to breaking Bell's inequality. When they subtract four photons they find that they are able to gain an slight increase in the Bell parameter, but at the cost of having to do four photon subtractions, a process which is associated with a very low probability of success.

This is the same low probability of success associated with conditional generation that we are faced with in our protocol. A way to avoid the could be to introduction a continuous variable quantum memory. Such a memory was recently experimentally realized by the group of E. Polzik [34].

Garcia-Patron et al. found that a one photon subtraction would produce a state incapable of breaking Bell. The process of subtracting one photon can though still increase the entanglement of the state. This was found both theoretically and experimentally by Ourjoumtsev et al. [35].

Others

There is a lot of activity in the field, very recently an experimental purification of coherent states [36], using a argumentation not far from the one presented here, where successfully presented. A purification protocol that is able to remove phase noise on a set of non-classical states are presented and experimentally demonstrated by A. Franzen et al. [37]. Our task in this thesis is somewhat more difficult, we try to remove Gaussian noise.

We have try to compare the ideas of this thesis to what other people previously have done. We have argued that this idea has advantages over some of the previous work, but we would like to point out that this is not the same as having better results. All the purification protocols cited have found better results that what we found here.

7.11 Summary

We have implemented a realistic model of the purification procedure suggested in the previous chapter. The calculations are done using Mathematica and a largely just linear algebra. We have used the Mathematica programs to search the phase space for optimal values for the phases applyed to the modes, phases used in the homodyne measurement and what value to condition on, in the homodyne projection.

We found that the best results are found for conditioning on measuring $X_0 = 0$ when performing the homodyne projection, which we were also able to make an argument for.

To perform the purification protocol two TMPS states are needed, the probability of generating such a set is very low. We could in principle achieve a higher level of success by using a quantum memory for light.

We have seen that iterating our purification protocol one time will produce the expected purification for low values of squeezing. Doing a second iteration repeats this conclusion, with a slight increase in the peak Bell-parameter. The gain in Bell parameter for each iteration of the purification protocol is however not impressive.

We outlined some of the other research being performed within this field, in order to compare the work presented in this thesis to the frontline research. We found that our protocol in princible has some distinct advantages over some of these. We condition on a ”click“ in our photo-detector, instead of ”no-click“ as done in [33]. We try to solve the harder problem of removing Gaussian noise, instead of just phase noise [37]. But as both these protocols are more successful it seems that the price of doing things right is to not be successful.

But there is hope, we use a procedure very similar to [36] who is able to successfully purify coherent states. So maybe the trouble is that we tryed to purify a state that was already to pure.

Chapter 8

Conclusion and Outlook

In this chapter we summarize and conclude the results which have been presented and discussed in chapter 5, 6 and 7. We also outline future work that could be done to further investigate and improve upon the suggested purification protocol.

8.1 Conclusion

We have presented the two mode photon subtracted (TMPS) state, and seen that it is an experimental feasible candidate for a loophole-free Bell test [8, 30]. The TMPS state is constructed by mixing a two mode squeezed vacuum state with non-squeezed vacuum on two unbalanced beamsplitters and conditionally subtracting a photon from each mode, see figure 5.1. It was found that with a realistic choice of parameters, Bell violations in the percent range could be achieved in a matter of hours, thus definitively disproving local realism.

We calculated the joint probability (JP) distribution for a set of quadrature phase measurements, for the TMPS state: $P(X_{A,\theta_j}, X_{B,\phi_k})$. We found that it was possible to choose phases (θ_j, ϕ_k) such that the JP distribution showed a high degree of correlations in the signs of the quadrature operators, see 5.5.

We found that when looking at the signs of the quadratures in the JP distribution, the TMPS state could too a good approximation be described as similar to the maximally entangled $|\phi^+\rangle$ Bell state. The TMPS state thus has properties that make it a good choice for an entanglement distribution source, and therefore interesting to find a purification protocol for.

A purification protocol for $|\phi^+\rangle$ Bell state exists [9]. It works in the following way: Alice and Bob apply phases to their qubit pairs and then perform cNOT measurements. If

their measurements agree they know that no error has occurred and they keep the resulting qubit pair.

We wanted to make a continuous variable counterpart to this purification protocol that should work on the TMPS states. The phase change is easy to do, but we need a continuous variable version of a cNOT measurement. We find that using a balanced beamsplitter and performing homodyne measurement of the quadratures does exactly this. We condition on measuring the same value, X_0, in both homodyne measurements. We have argued that these steps should lead to a purification of the TMPS states.

To calculate what the effect of the purification protocol actually is, we have written multiple programs in Mathematica. Most of the calculations can be done using only linear algebra, but some numerical integration is also implemented. We have set up the programs so that we are free to explore the entire phase space and we find that the results are best for X_0 equal to zero, see figure 7.3. The applyed phases are also optimized.

For the choice $X_0 = 0$ the calculations simplifies further and we can do all calculations using only linear algebra. This enables us to calculate the effect of a repetition of the protocol.

We find the result of the protocol summarized in figure 7.8. We see that for a low squeezing parameter, $\lambda \in [0.4, 0.5]$, the protocol works. The purified state shows a higher Bell parameter then the initial TMPS state when comparing for the same amount of initial squeezing λ. We are even able to produce steps capable of breaking Bell's inequality that before purification where uncapable.

The highest achievable Bell parameter for the one time and two time purified state have not been found to be higher than what we got from the TMPS state, in the percent range. We are not able to produce states that exhibit a stronger entanglement than the optimal initial state, but we are able to improve upon a range of initial states with a lower than optimal squeezing.

When we implement the purification we need two copies of the TMPS state. We have calculated the initial probability of successful generation of one TMPS state, P_G, the probability of preparing two such states are given as P_G^2. We are therefore left with a very low successrate in preparing the states needed for the purification protocol. The purification protocol itself is not dependent on this, but rather on the probability of measuring the same quadrature X_0 in mode.

In summary. We have constructed a continuous variable purification protocol using ideas from D. Deutsch et al. [9] for the purpose of purifying TMPS states. We found that the purification protocol works when it is applied to TMPS states with a lower than optimal squeezing parameter. The gain in Bell parameter is to be seen in the light of

the probabilities associated with the initial generation of the needed states. We have not successfully produced a method to achieve a better loophole-free test of Bell's inequality than suggested in [8, 30, 31], but the method has seen reasonably success in purifying less than optimal TMPS states.

8.2 Outlook

Much can still be done to further explore the properties of the suggested purification protocol.

Firstly. It is desirable to investigate the effect of conditioning on a broad range of homodyne measurement. It would be interesting to see how the purification would function if $X_{0,new} \in [X_0 - \epsilon, X_0 + \epsilon]$. When we conditioned on a single value for X_0 then probability of a successful implementation of the purification protocol drops to 0. It would be very interesting to know how this probability would behave for $X_{0,new} \in [X_0 - \epsilon, X_0 + \epsilon]$.

Secondly. When we did the second iteration of the purification protocol we found a slight increase in the highest achievable Bell violation as compared to what we found for one iteration. It would be very interesting to see what happened after one more iteration. It would be a relatively simple task to repeat the protocol one more time, the biggest trouble would be the time it will take to simulate the behavior of the three time purified state, as this would involve 256^2 terms.

Third and last. It would be interresting to further investigate the possibilities of implementing quantum memories to improve the successrate of the generation of initial states for the purification protocol.

In summery. Much can still be done to investigate the properties of the purification protocol. It is in particular desirable to see the effect on conditioning on a range of values when doing the conditioning homodyne detection.

Appendix A

Gaussian integral

In this appendix we will prove a theorem that is used many times throughout this thesis. It states that given a vector $\vec{r} = [\vec{x}, \vec{y}]^T = [x_1, \ldots, x_n, y_1, \ldots, y_m]^T$ of dimension $n + m$ and a symmetric $[(n + m) \times (n + m)]$-matrix of the form

$$M = \begin{bmatrix} A[n \times n] & C[n \times m)] \\ C^T[m \times n] & B[m \times m] \end{bmatrix}, \tag{A.1}$$

then the following is true

$$\int d\vec{y} \exp[-\vec{r}^T M \vec{r}] = \sqrt{\frac{\pi^m}{\det[B]}} \exp[-\vec{x}^T (A - CB^{-1}C^T)\vec{x}]. \tag{A.2}$$

We want to calculate the following integral over all y_k coordinates.

$$\int d\vec{y} \exp[-\vec{r}^T M \vec{r}] \tag{A.3}$$

where $d\vec{y} = dy_1 \cdots dy_m$. First we do a substitution in the integration, introducing $\vec{u} = [u_1, \ldots u_m]^T$ which is given as

$$\vec{u} = \vec{y} + B^{-1}C^T\vec{x} \qquad \text{and} \qquad \vec{u}^T = \vec{y}^T + \vec{x}^T C B^{-1} \tag{A.4}$$

where we see that $du_k = dy_k$ for $k = 1 \ldots m$. Rewriting the exponent in term of the submatrices defined above, we see that

$$\vec{r}^T M \vec{r} = \vec{x}^T A \vec{x} + \vec{x}^T C \vec{y} + \vec{y}^T C^T \vec{x} + \vec{y}^T B \vec{y}. \tag{A.5}$$

We now get the idea to perform the calculation

$$\vec{u}^T B\vec{u} = \vec{x}^T CB^{-1}C^T\vec{x} + \vec{x}^T C\vec{y} + \vec{y}^T C^T\vec{x} + \vec{y}^T B\vec{y}, \tag{A.6}$$

and we see that

$$\vec{r}^T M\vec{r} = \vec{u}^T B\vec{u} + \vec{x}^T(A - CB^{-1}C^T)\vec{x} \tag{A.7}$$

So we can now write a simpler integral, using $d\vec{u} = du_1 \dots du_m$

$$\int d\vec{y}\exp[-\vec{r}^T M\vec{r}] = \exp[-\vec{x}^T(A - CB^{-1}C^T)\vec{x}] \int d\vec{u}\exp[-\vec{u}^T B\vec{u}] \tag{A.8}$$

As M where assumed symmetric we know that it is possible to make a shift of basis to put the exponent in diagonal form. We define $\vec{v} = U\vec{u}$ and $d\vec{v} = d\vec{u}$, yielding

$$\int d\vec{u}\exp[-\vec{u}^T B\vec{u}] = \int d\vec{v}\exp[-\vec{v}^T UBU^{-1}\vec{v}]. \tag{A.9}$$

The different diagonal elements are labeled e_k, and we can write

$$\int d\vec{v}\exp[-\vec{v}^T UBU^{-1}\vec{v}] = \int d\vec{v}\exp[-\sum_{k=1}^{m} e_k v_k^2]. \tag{A.10}$$

The integral is now easy to calculate,

$$\int d\vec{v}\exp[-\sum_{k=1}^{m} e_k v_k^2] = \sqrt{\frac{\pi^m}{e_1 \cdots e_m}}. \tag{A.11}$$

Utilizing that $e_1 \cdots e_m = \det[UBU^{-1}] = \det[B]$, we finally arrive at the formulation that we wanted

$$\int d\vec{y}\exp[-\vec{r}^T M\vec{r}] = \sqrt{\frac{\pi^m}{\det[B]}}\exp[-\vec{x}^T(A - CB^{-1}C^T)\vec{x}]. \tag{A.12}$$

We have only assumed that M was symmetric, this is a inherent property in covariance matrices.

Appendix B

Wigner functions for vacuum and for the identity matrix

The calculation of the Wignerfunctions of vacuum $|0\rangle\langle 0|$ and for the identity matrix I, are done by straight forward implementation of the definition of the Wignerfunction.

B.1 Wigner function for the identity matrix

Starting by doing the calculation for the identity matrix for a single mode, we find that

$$W_I = \frac{1}{2\pi}\int dx' \langle X - x'/2|I|X + x'/2\rangle \exp[iPx']. \tag{B.1}$$

The position kets are orthogonal, so this reduce to performing the integral

$$W_I = \frac{1}{2\pi}\int dx' \delta(x') \exp[iPx'] = \frac{1}{2\pi}. \tag{B.2}$$

This is the result for one vacuum mode. For two vacuum modes the Wigner function is simply $(2\pi)^{-2}$, and so fourth.

B.2 Wigner function for the vacuum operator

Again we start with the definition

$$W_{|0\rangle\langle 0|} = \frac{1}{2\pi}\int dx' \langle X - x'/2|0\rangle\langle 0|X + x'/2\rangle \exp[iPx'] \tag{B.3}$$

This is simply the Wigner function for the groundlevel of a harmonic oscillator. We know the representation of the ground level in a harmonic oscillator in the position basis. Given in dimensionless coordinates this is $\langle x|0\rangle = \pi^{-1/4}\exp[-1/2x^2]$.

Using this we see that

$$\begin{aligned} W_{|0\rangle\langle 0|} &= \frac{1}{2\pi}\int dx'\pi^{-1/2}\exp[-1/2[(X-x'/2)^2+(X+x'/2)^2]]\exp[iPx'] \\ &= \frac{1}{2\pi}\pi^{-1/2}\exp[-X^2]\int dx'\exp[-1/4x'^2]\exp[iPx']. \end{aligned} \tag{B.4}$$

Cauchy's integral formula gives the identity

$$\int dt\exp[-\frac{1}{2}t^2]\exp[ibt] = \sqrt{2\pi}\exp[-\frac{1}{2}b^2], \tag{B.5}$$

this can be used here. After a change of variables $x = \sqrt{2}t$, we arrive at

$$W_{|0\rangle\langle 0|} = \frac{1}{\pi}\exp[-(X^2+P^2)]. \tag{B.6}$$

With a vector $r = [X,P]^T$ we can see that this can be written as

$$W_{|0\rangle\langle 0|} = \frac{1}{\pi}\exp[-r^T I r] \tag{B.7}$$

The equation above is easy to implement in a matrix formalism.

Appendix C

Plot of the effect of the purification protocol

Below are shown plots of the effect of the purification protocol for two additional values of T. Its is clear that the effect of the purification is not as pronounced for lower values of T than the results shown in the main part of the thesis, that is, for T = 0.99.

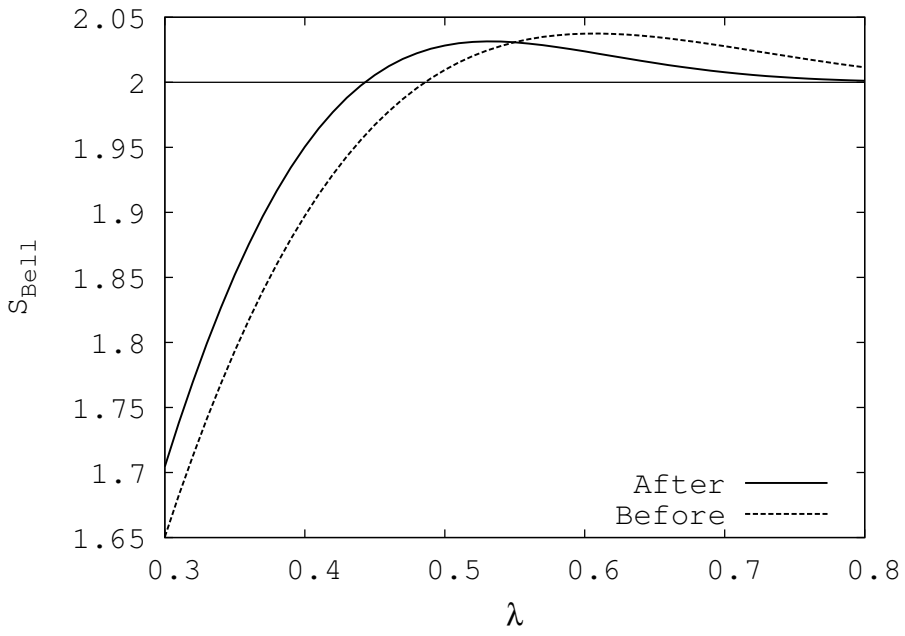

Figure C.1: *Plot of the effect on the purification protocol. The results shown are for T = 0.95 and X0=0.*

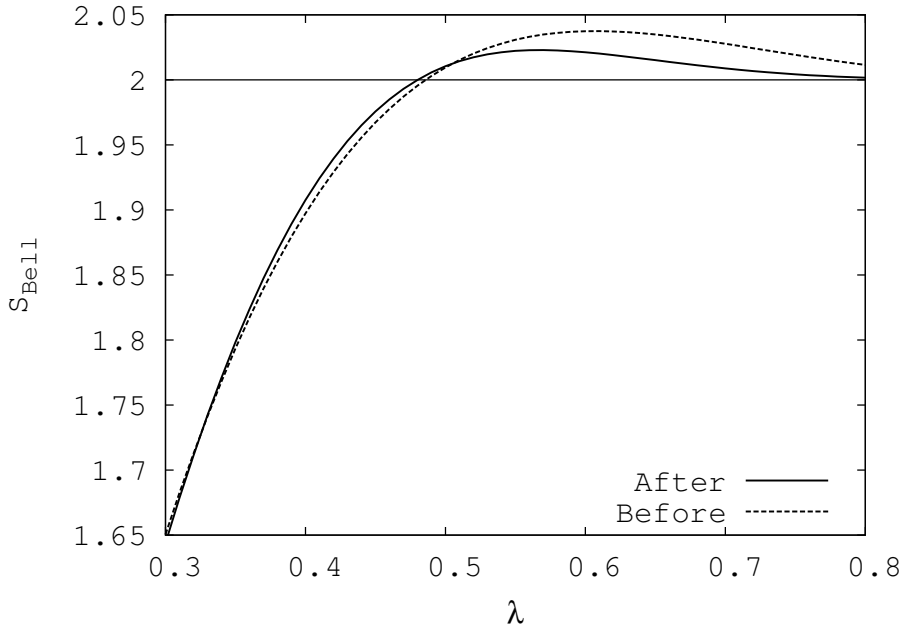

Figure C.2: *Plot of the effect on the purification protocol. The results shown are for T = 0.90 and X0=0.*

Appendix D

List of programs

In this appendix we list the Mathematica notebooks that we have used in obtaining the numerical and analytical results in this thesis. The total amount of code is too considerable to allow for a print out to be included.

The programs will be suplied if a request is made to *mads.lykke@gmail.com*, they are not yet commented thouroughly, but I will be happy to address any questions regarding their inner workings.

The following programs have been used in this thesis:

TwoModePhotonSubtractedState.nb Calculates all the properties of the TMPS state, it is possible to vary all parameters and the results are either plotted or written to a data file.

OneTimePurifiedStateX0eqaulto0.nb Calculates all the properties of the purified state. This program only calculates the case of $X_0 = 0$, but it is possible to vary all other parameters in the purification procedure and for the two TMPS states that are used. Results are either plotted or written to a data file.

OneTimePurifiedStateX0not0.nb Calculates all the properties of the purified state. In this program it is possible to vary all parameters in the purification procedure and for the two TMPS states that are used. The possibility of also varying X_0 slows down the calculations significantly as numerical calculations occur. Results are either plotted or written to a data file.

TwoTimePurifiedStateX0equalto0.nb Calculates all the properties of the two time purified state. This program only calculates the case of $X_0 = 0$, but it is possible to vary all other parameters in the purification procedure and for the four TMPS states that are used. Results are either plotted or written to a data file.

PlotDATA.nb This function select data from a data file generated by one of the above mentioned programs and either plot it or make a new file that is to be used in gnuplot.

Bibliography

[1] B. Podolsky A. Einstein and N. Rosen. Can quantum-mechanical description of physical reality be considered complete? *Phys. Rev.*, 47:777–, 1935.

[2] J.S. Bell. On the Eistein Podolsky Rosen paradox. *Physics 1*, 1964.

[3] J.S. Bell. On the problem of hidden variables in quantum mechanics. *Rev. Mod. Phys.*, 38:447, 1966.

[4] Alain Aspect, Jean Dalibard, and Gérard Roger. Experimental test of Bell's inequalities using time- varying analyzers. *Phys. Rev. Lett.*, 49(25):1804–1807, Dec 1982.

[5] Alain Aspect, Philippe Grangier, and Gérard Roger. Experimental realization of Einstein-Podolsky-Rosen-Bohm gedankenexperiment: A new violation of Bell's inequalities. *Phys. Rev. Lett.*, 49(2):91–94, Jul 1982.

[6] Alain Aspect, Philippe Grangier, and Gérard Roger. Experimental tests of realistic local theories via Bell's theorem. *Phys. Rev. Lett.*, 47(7):460–463, Aug 1981.

[7] Peter W. Shor. Polynomial-time algorithms for prime factorization and discrete logarithms on a quantum computer. *SIAM J.Sci.Statist.Comput.*, page 1484, 1997.

[8] R. García-Patrón, J. Fiurášek, N. J. Cerf, J. Wenger, R. Tualle-Brouri, and Ph. Grangier. Proposal for a loophole-free Bell test using homodyne detection. *Phys. Rev. Lett.*, 93(13):130409, Sep 2004.

[9] David Deutsch, Artur Ekert, Richard Jozsa, Chiara Macchiavello, Sandu Popescu, and Anna Sanpera. Quantum privacy amplification and the security of quantum cryptography over noisy channels. *Phys. Rev. Lett.*, 77(13):2818–2821, Sep 1996.

[10] S. Barnett and P.M. Radmore. *Methods in Theoretical Quantum Optics*. Methods in Theoretical Quantum Optics, 1997.

[11] C.C. Gerry and P.L. Knight. *Introductory Quantum Optics*. Cambridge University Press, 2005.

[12] M.O. Scully and M.S. Zubairy. *Quantum optics*. Cambridge University Press, 1997.

[13] J.J. Sakurai. *Modern Quantum Mechanics*. Addison-Wesley Publishing Company, revised edition edition, 1994.

[14] Eugen Merzbacher. *Quantum Mechanics*. John Wiley & Sons, Inc., 1998.

[15] J.S. Bell. *Speakable and Unspeakable in Quantum Mechanics*. Cambridge University Press, 2nd. edition, 2004.

[16] Michael A. Nielsen and Isaac L. Chuang. *Quantum Computation and Quantum Information*. Cambridge University Press, 2000.

[17] John Preskill. Quantum information and computation. Lecture Notes for Physics 229, California Institure of Technology, September 1998.

[18] John F. Clauser, Michael A. Horne, Abner Shimony, and Richard A. Holt. Proposed experiment to test local hidden-variable theories. *Phys. Rev. Lett.*, 23(15):880–884, Oct 1969.

[19] David J. Griffiths. *Introduction to Electrodynamics*. Prentice-Hall, 3rd ed. edition, 1999.

[20] John David Jackson. *Classical Electrodynamics*. Wiley, third edition edition, 1999.

[21] D. Deutsch. Quantum theory, the Church-Turing principle and the universal quantum computer. *Proc. R. Soc. Lond. A*, 1985.

[22] David Deutsch; Richard Josza. Rapid solution of problems by quantum computing. volume 439. The Royal Society, 1992.

[23] R.P.Feynmann. Simulating physics with computers. *Int. J. Theor. Phys.*, 21, 1982.

[24] M.O. Scully M. Hillery, R.F. O'Connell and E.P. Wigner. Distribution functions in physiscs: fundamentals. *Physics report*, 106(3):121–, 1984.

[25] R. Simon and E.C.G. Sudarshan. Gaussian-Wigner distributions in quantum mechanics and optics. *Physical Review A.*, 36(8):3868–3880, 1987.

[26] J. Perina. *Quantum Statistics of Linear and Nonlinear Optical Phenomena*. Kluwer Academic Publisher, 2nd. edition, 1991.

[27] J. Eisert, S. Scheel, and M. B. Plenio. On the impossibility of distilling Gaussian states with Gaussian operations. *Physical Review Letters*, 89:137903, 2002.

[28] Jaromír Fiurášek. Gaussian transformations and distillation of entangled Gaussian states. *Phys. Rev. Lett.*, 89(13):137904, Sep 2002.

[29] Géza Giedke and J. Ignacio Cirac. Characterization of Gaussian operations and distillation of Gaussian states. *Phys. Rev. A*, 66(3):032316, Sep 2002.

[30] Hyunchul Nha and H. J. Carmichael. Proposed test of quantum nonlocality for continuous variables. *Phys. Rev. Lett.*, 93(2):020401, Jul 2004.

[31] Raúl García-Patrón, Jaromír Fiurášek, and Nicolas J. Cerf. Loophole-free test of quantum nonlocality using high-efficiency homodyne detectors. *Phys. Rev. A*, 71(2):022105, Feb 2005.

[32] H.X. Lu Y. Kang and Y.-H. Lo. Dark count probability and quantum efficiency of avalanche photodioses for sigle-photon detection. *Applied Physics Letters*, 83(14):2955–2957, 2203.

[33] Sonja Daffer and Peter L. Knight. Generating optimal states for a homodyne Bell test. *Phys. Rev. A*, 72(3):034101, Sep 2005.

[34] Brian Julsgaard, Jacob Sherson, J. Ignacio Cirac, Jaromir Fiurasek, and Eugene S. Polzik. Experimental demonstration of quantum memory for light. *Nature*, 432:482, 2004.

[35] Alexei Ourjoumtsev, Aurelien Dantan, Rosa Tualle-Brouri, and Philippe Grangier. Increasing entanglement between Gaussian states by coherent photon subtraction. *Physical Review Letters*, 98(3):030502, 2007.

[36] Ulrik L. Andersen, Radim Filip, Jaromir Fiurasek, Vincent Josse, and Gerd Leuchs. Experimental purification of coherent states. *Physical Review A*, 72:060301, 2005.

[37] Alexander Franzen, Boris Hage, James DiGuglielmo, Jaromír Fiurás˘ek, and Roman Schnabel. Experimental demonstration of continuous variable purification of squeezed states. *Phys. Rev. Lett.*, 97(15):150505, Oct 2006.